Article

Cancer Cell

A Potent and Selective Small-Molecule Degrader of STAT3 Achieves Complete Tumor Regression *In Vivo*

Graphical Abstract

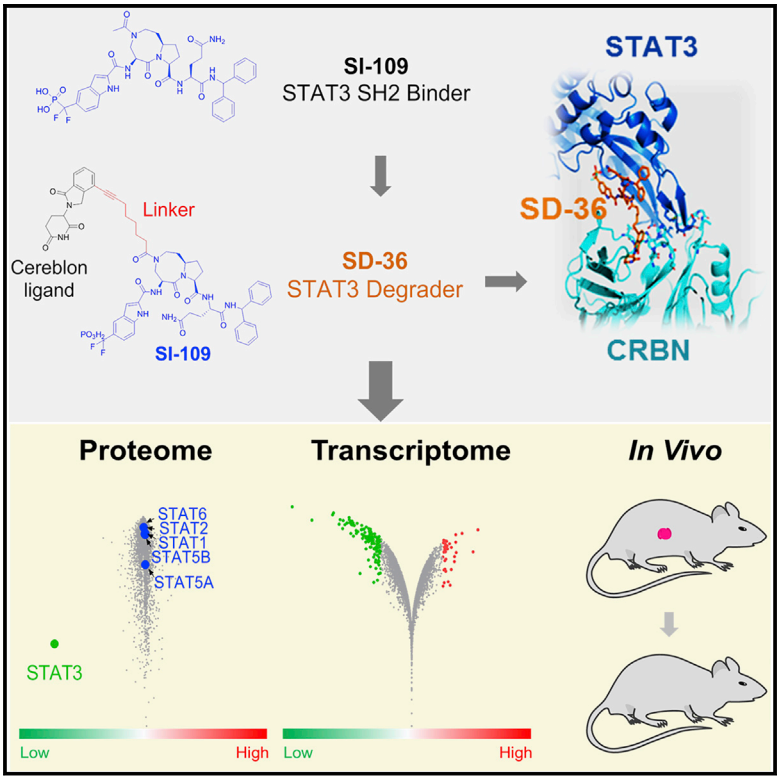

Highlights

- SD-36 selectively degrades STAT3 over other STAT proteins
- SD-36 exerts growth inhibitory activities in leukemia and lymphoma cell lines
- SD-36 achieves complete and long-lasting tumor regression in mouse tumor models
- SD-36 is well tolerated in immune competent mice

Authors

Longchuan Bai, Haibin Zhou, Renqi Xu, ..., Duxin Sun, Jeanne A. Stuckey, Shaomeng Wang

Correspondence

shaomeng@umich.edu

In Brief

Bai et al. develop SD-36, a proteolysis targeting chimera (PROTAC) that selectively degrades STAT3 and inhibits the growth of leukemia and lymphoma cell lines. SD-36 is well tolerated in immune-competent mice and induces durable tumor regression *in vivo* in xenograft models.

Bai et al., 2019, Cancer Cell *36*, 498–511
November 11, 2019
https://doi.org/10.1016/j.ccell.2019.10.002

CellPress

CellPress

Cancer Cell
Article

A Potent and Selective Small-Molecule Degrader of STAT3 Achieves Complete Tumor Regression *In Vivo*

Longchuan Bai,[1,2,8] Haibin Zhou,[1,2,8] Renqi Xu,[1,2,8] Yujun Zhao,[1,2,8] Krishnapriya Chinnaswamy,[5] Donna McEachern,[1,2] Jianyong Chen,[1,2] Chao-Yie Yang,[1,2] Zhaomin Liu,[1,2] Mi Wang,[1,2] Liu Liu,[1,2] Hui Jiang,[1,3] Bo Wen,[1,4] Praveen Kumar,[1,4] Jennifer L. Meagher,[5] Duxin Sun,[1,4] Jeanne A. Stuckey,[1,5] and Shaomeng Wang[1,2,6,7,9,*]

[1]Rogel Cancer Center, University of Michigan, Ann Arbor, MI 48109, USA
[2]Department of Internal Medicine, University of Michigan, Ann Arbor, MI 48109, USA
[3]Department of Biostatistics, University of Michigan, Ann Arbor, MI 48109, USA
[4]Department of Pharmaceutical Sciences, University of Michigan, Ann Arbor, MI 48109, USA
[5]Life Sciences Institute, University of Michigan, Ann Arbor, MI 48109, USA
[6]Department of Pharmacology, University of Michigan, Ann Arbor, MI 48109, USA
[7]Department of Medicinal Chemistry, University of Michigan, Ann Arbor, MI 48109, USA
[8]These authors contributed equally
[9]Lead Contact
*Correspondence: shaomeng@umich.edu
https://doi.org/10.1016/j.ccell.2019.10.002

SUMMARY

Signal transducer and activator of transcription 3 (STAT3) is an attractive cancer therapeutic target. Here we report the discovery of SD-36, a small-molecule degrader of STAT3. SD-36 potently induces the degradation of STAT3 protein *in vitro* and *in vivo* and demonstrates high selectivity over other STAT members. Induced degradation of STAT3 results in a strong suppression of its transcription network in leukemia and lymphoma cells. SD-36 inhibits the growth of a subset of acute myeloid leukemia and anaplastic large-cell lymphoma cell lines by inducing cell-cycle arrest and/or apoptosis. SD-36 achieves complete and long-lasting tumor regression in multiple xenograft mouse models at well-tolerated dose schedules. Degradation of STAT3 protein, therefore, is a promising cancer therapeutic strategy.

INTRODUCTION

Signal transducer and activator of transcription 3 (STAT3), a member of the STAT family, is a latent transcription factor that is activated in response to various cytokines, growth factors, and oncogene signals. STAT3 is constitutively activated in various human cancers, and its activation is frequently associated with poor prognosis (Banerjee and Resat, 2016; Haura et al., 2005; Johnson et al., 2018; Yu and Jove, 2004). As a transcription factor, STAT3 regulates a set of genes implicated in cancer cell survival, proliferation, angiogenesis, invasion, metastasis, drug resistance, and immune evasion (Haura et al., 2005; Lee et al., 2011; Yu and Jove, 2004; Zhao et al., 2016). A large body of cumulative evidence strongly supports STAT3 as an attractive therapeutic target in cancer and other human diseases.

It was originally hypothesized that phosphorylation of STAT3 at Tyr705 is essential for its dimerization and the subsequent transactivation of target genes. STAT3 dimerization occurs through the interaction of a phosphopeptide-containing pTyr705 from one monomer with the binding pocket in the Src-homology 2 (SH2) domain of another monomer. Consequently, inhibitors of the STAT3 SH2 domain would prevent dimerization and transcriptional activity of STAT3, and this has been a focus of development of STAT3 inhibitors. Although three small-molecule inhibitors of the STAT3 SH2 domain have reached the clinical development stage, they demonstrated very limited clinical activity (Johnson et al., 2018). One major issue with STAT3 SH2

Significance

STAT3 has been intensely pursued as a therapeutic target for human cancer and other diseases, but targeting STAT3 with small molecules has been challenging. Here we report the discovery of SD-36 as a potent and selective small-molecule degrader of STAT3 proteins. SD-36 potently and selectively degrades STAT3 over other STAT proteins and exerts robust anti-tumor activity in preclinical models of acute myeloid leukemia and anaplastic large-cell lymphoma. Our study demonstrates that targeted degradation of STAT3 is a promising therapeutic strategy for cancer.

domain inhibitors is that STAT3 and other STAT family members share a highly structurally homologous SH2 domain, making it difficult to obtain highly selective STAT3 inhibitors. A second major issue is that monomeric STAT3 protein also has transcriptional activity (Yang and Stark, 2008), so inhibitors of the STAT3 SH2 domain that block STAT3 dimerization are predicted to only partially suppress the gene transcriptional activity of STAT3.

Recently, proteolysis targeting chimera (PROTAC) technology has gained momentum for its promise for the development of a type of therapeutics that induces targeted protein degradation (Pettersson and Crews, 2019). Here we aimed to develop a potent and specific PROTAC degrader of STAT3 and evaluate its therapeutic potential for cancer.

RESULTS

Structure-Based Design of Potent and Cell-Permeable Inhibitors of the STAT3 SH2 Domain

Based on our previous STAT3 SH2 domain inhibitor CJ-887 (compound **1**) (Chen et al., 2010a), we have performed extensive optimization, as summarized in Figure 1A, to obtain potent and cell-permeable STAT3 inhibitors. First, we designed compound **2** by cyclization of the amino group with the phenyl group to form an indole, which binds to STAT3 with a K_i value of 39 nM (Figures S1A–S1C), but is also ineffective in suppressing STAT3 activity in cells. We reasoned that the phosphate group in compound **2** is largely responsible for its inactivity in cells. Accordingly, we replaced the phosphate group of compound **2** with difluoromethylphosphonic acid, which has been used to mimic the phosphate group (Smyth et al., 1992), yielding compound **3**. Compound **3** binds to STAT3 protein with a K_i value of 7 nM, 5 times more potent than compound **2**. Computational models of compound **3** in complex with STAT3 showed that its eight-membered ring is exposed to the solvent environment (Figure S1D). To facilitate the design of STAT3 degraders, we replaced one of the carbon atoms of the eight-membered ring with nitrogen and synthesized compound **4** (SI-108) and compound **5** (SI-109), with N-methyl and N-acetyl substituents, respectively. Both SI-108 (K_i = 11 nM) and SI-109 (K_i = 9 nM) bind to STAT3 with high affinities. In our cell-based functional assay, SI-109 and SI-108 effectively inhibited the transcriptional activity of STAT3 in a STAT3-luciferase reporter assay (half maximal inhibitory concentration [IC_{50}] ~3 μM, Figure S1E). Therefore, our efforts have yielded high-affinity and cell-permeable STAT3 SH2 domain inhibitors.

Design of PROTAC STAT3 Degraders

Cereblon (CRBN)/cullin 4A and von Hippel-Lindau (VHL)-1/cullin 2 E3 ligase complexes have been successfully employed for the design of PROTAC degraders for different proteins (Bondeson and Crews, 2017; Lai and Crews, 2017; Neklesa et al., 2017; Paiva and Crews, 2019). Therefore, we have designed putative STAT3 degraders using our STAT3 inhibitors SI-109 and SI-108 and ligands for CRBN or VHL. Our initial data identified SD-36 (compound **6**) as a potent STAT3 degrader (Figure 1B). SD-36 was designed using an analog of CRBN ligand lenalidomide and the STAT3 inhibitor SI-109. To facilitate the investigation of the mechanism of action of SD-36, we also synthesized SD-36Me (compound **7**) (Figure 1B), in which a methyl group was installed to block binding to CRBN (Fischer et al., 2014; Lu et al., 2015). A fluorescence polarization binding assay showed that lenalidomide-conjugated SD-36, inactive control SD-36Me and SH2 domain inhibitors SI-109 and SI-108 have comparable high affinities with recombinant STAT3 protein, with K_i values of 11, 20, 9, and 11 nM, respectively (Figure S1C).

To elucidate the structural basis for the strong binding affinities of our designed STAT3 inhibitors and degraders, we determined the co-crystal structures of SI-109 (PDB: 6NUQ) and SD-36 (PDB: 6NJS) complexed with the STAT3 SH2 domain (Figure 1C). Our co-crystal structures show that SI-109 and SD-36 bind to STAT3 in nearly identical binding modes. Both compounds mimic the binding of the STAT3 phosphotyrosine peptide. Specifically, the phosphoric acid moiety of SD-36 forms an extensive hydrogen bonding network with the side chains of Arg609, Ser611, and Ser613, and the backbone amide nitrogens of Glu612 and Ser613. The pro-(*S*)-F atom of the difluoromethyl forms a strong hydrogen bond with Arg609. The indole group lies across a shallow cleft formed between Pro639 and Ser636. The glutamine group in SD-36 forms bifurcated hydrogen bonds with the side chain of Gln644 and its carbonyl group forms water-mediated hydrogen bonds with the hydroxyl of Tyr640 and the amide nitrogen of Lys658. The pro-(*S*)-phenyl group of the diphenylmethyl group sits on top of a large hydrophobic pocket formed by Leu666, Met660, and Ile659. The [8,5] bicyclic ring system does not appear to have specific interactions with the protein, but is tethered on either side by hydrogen bonds: the backbone amide nitrogen between the bicyclic ring and the indole forms a hydrogen bond with the backbone of Ser636, while the backbone carbonyl group between the five-membered ring and glutamine in SD-36 forms a hydrogen bond with Tyr657. Therefore, the conformational constraint of the bicyclic ring system provides an ideal conformation to orient the difluoromethylphosphonic acid and the glutamine moieties to form optimal interactions with STAT3.

These co-crystal structures (PDB: 6NUQ, 6NJS.) provide a structural basis for their high binding affinities to STAT3.

SD-36 Is a Potent and *Bona Fide* PROTAC Degrader of STAT3 Protein

We evaluated SD-36 for its ability to degrade the STAT3 protein in human cells. SD-36 treatment resulted in a time- and concentration-dependent depletion of total STAT3 protein in all the human cell lines tested, with representative data shown for acute myeloid leukemia (AML) cell line MOLM-16 and anaplastic large-cell lymphoma (ALCL) cell lines SU-DHL-1, DEL, and KI-JK (Figures 2A, 2B, and S2A). For example, 250 nM SD-36 depleted >90% of STAT3 protein in MOLM-16 cells after 4 h treatment and >50% of STAT3 protein in DEL, KI-JK, and SU-DHL-1 cells after 7 h treatment (Figures 2B and S2A). In comparison, the STAT3 inhibitors SI-109 and SD-36Me had no significant effect on the levels of STAT3 protein (Figure 2A). The classical "hook effect" for PROTAC degraders (Bondeson et al., 2015; Burslem et al., 2018a; Chan et al., 2018; Farnaby et al., 2019; Lu et al., 2015; Olson et al., 2018; Schiedel et al., 2018; Winter et al., 2017) was not observed for SD-36 at concentrations as high as 10 μM in all the cell lines tested (Figure 2A).

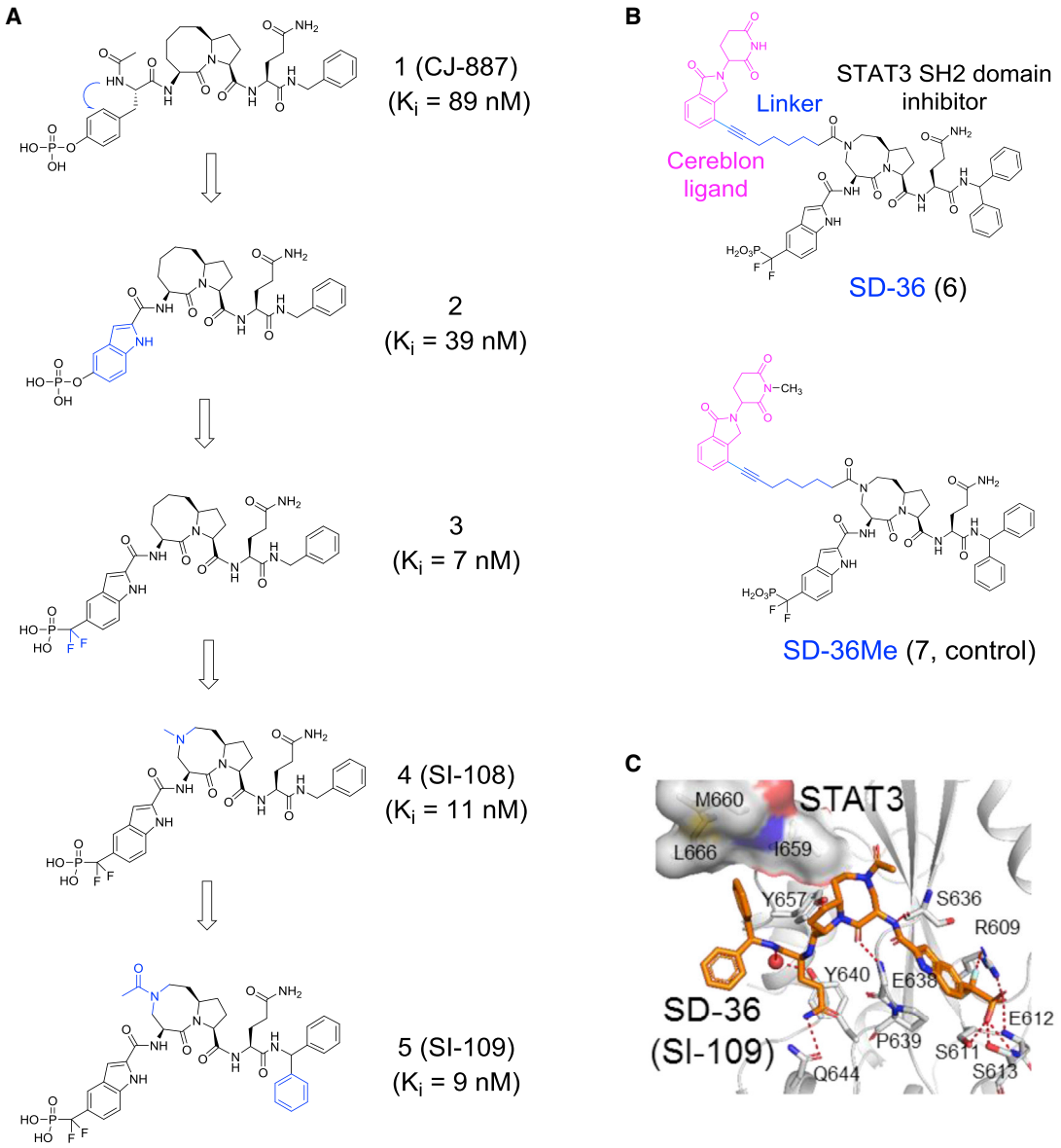

Figure 1. Structure-Guided Design of STAT3 SH2 Domain Inhibitors and PROTAC Degraders

(A) Design of STAT3 SH2 domain inhibitors. K_i values are the means of three independent experiments.

(B) Chemical structures of PROTAC STAT3 degrader SD-36 and its inactive control SD-36Me.

(C) Co-crystal structure of SD-36 (orange) with STAT3 (gray). SI-109 binds to STAT3 in nearly identical binding modes as SD-36. Key residues in STAT3 interacting with SD-36 are labeled and hydrogen bonds are depicted as red dashed lines. A mediating water molecule is shown as a sphere. The hydrophobic patch formed by I659, M660, and L666 is shown as surface representation.

See also Figure S1.

SD-36 effectively reduced the levels of activated pSTAT3 (Y705) with similar potencies in MOLM-16 cells (Figure 2B). SD-36 also efficiently degraded STAT3 protein in murine cells (Figure S2B).

Consistent with its PROTAC design, excess STAT3 SH2 inhibitor SI-108 or the CRBN ligand lenalidomide blocked SD-36-induced depletion of STAT3 protein (Figure S2C). Furthermore, both the proteasome inhibitor carfilzomib and the NEDD8-activating E1 enzyme inhibitor MLN4924 blocked SD-36-induced degradation of STAT3 (Figure S2C). In addition, knockdown of CRBN diminished SD-36-mediated STAT3 degradation in multiple cell lines (Figures 2C and S2D). These data demonstrate that SD-36 works as a *bona fide* PROTAC STAT3 degrader in cells.

Our co-crystal structure of SD-36 complexed with STAT3 (Figure 1C) shows that the head difluoromethylphosphonic acid group of SD-36 forms strong hydrogen bond interactions with Arg609, Ser611, and Ser613 in the SH2 domain of STAT3. Mutations of Arg609 or Ser611/Ser613 rendered the STAT3 protein resistant to degradation by SD-36 (Figure 2D), indicating that direct engagement of SD-36 with the STAT3 SH2 domain in cells is required for its induced STAT3 degradation.

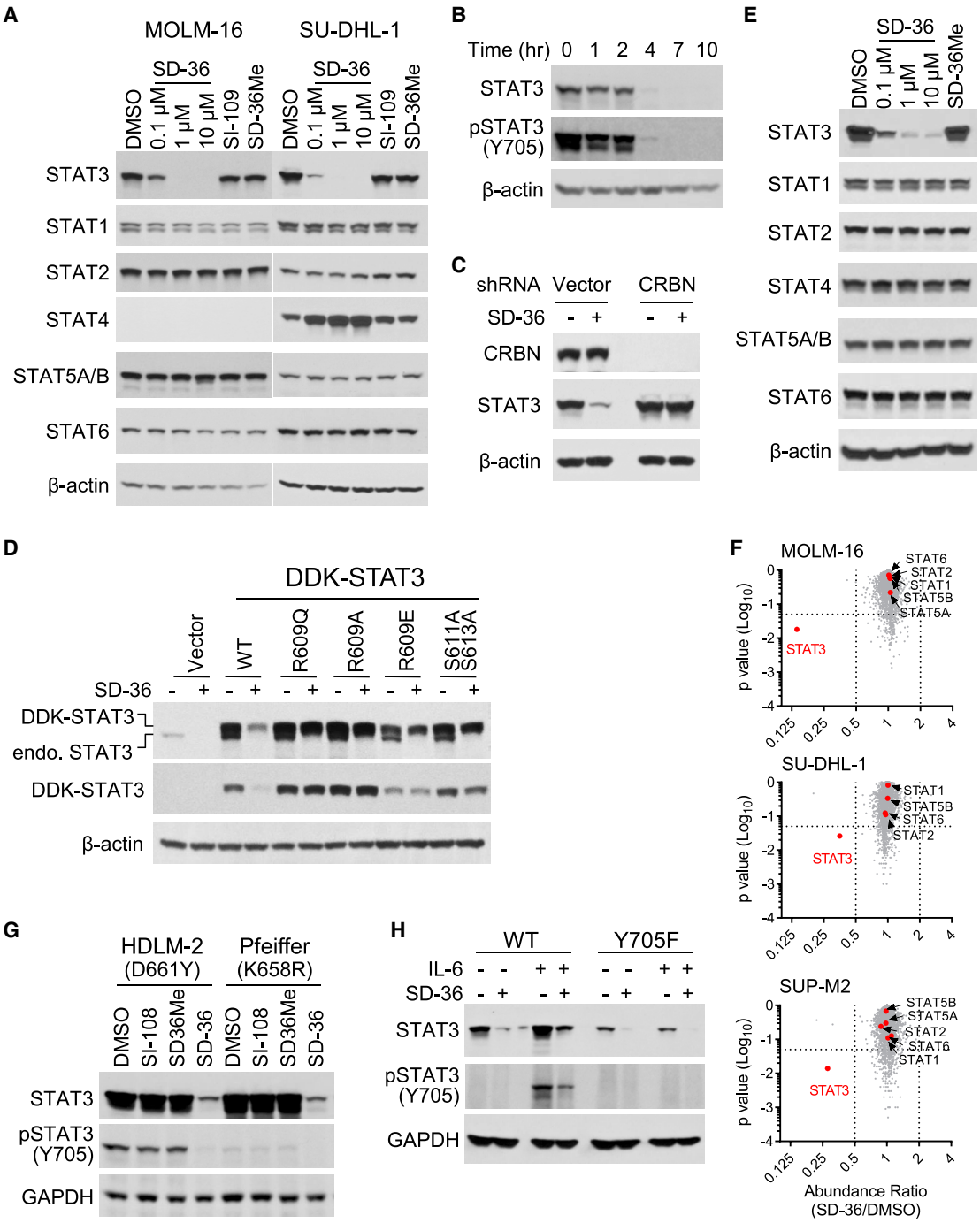

Figure 2. SD-36-Mediated Cellular STAT3 Protein Degradation

(A) Cells were treated with SD-36, 10 μM of SI-109 or SD-36Me for 3 h (MOLM-16) or 24 h (SU-DHL-1) for immunoblotting.

(B) MOLM-16 cells were treated with 0.25 μM of SD-36 for immunoblotting.

(C) MOLM-16 cells stably transduced with vector control or *CRBN* small hairpin RNAs were treated with 1 μM of SD-36 for 3 h for immunoblotting.

(D) MDA-MB-231 cells transfected with the indicated STAT3-expressing vectors were treated with 1 μM of SD-36 for 16 h for immunoblotting.

(E) Human PBMCs were treated with SD-36 or 10 μM of SD-36Me for 24 h for immunoblotting.

(F) Cells were treated with 10 μM of SD-36 for 2.5 h for multiplexed quantitative proteomics analysis. p value, Student's t test.

(G) Cells were treated with 1 μM of the indicated compounds for 24 h for immunoblotting.

(H) Parental DLD-1 (wild type [WT]) and DLD-1/STAT3$^{Y705F/Y705F}$ (Y705F) cells were pre-incubated with or without 10 ng/mL of interleukin-6 (IL-6) for 15 min, then 1 μM of SD-36 for 24 h for immunoblotting.

See also Figure S2.

SD-36 Achieves Extremely High Cellular Selectivity for Degradation of STAT3 over Other STATs

The STAT family has seven members, namely STAT1, STAT2, STAT3, STAT4, STAT5A, STAT5B, and STAT6, which share a highly conserved SH2 domain. The direct binding affinities of SI-109 and SD-36 to STAT3 and other STAT proteins were evaluated using a biolayer interferometry method (Figure S2E). SI-109 and SD-36 bind to STAT3 with K_d values of ~50 nM, and STAT1 and STAT4 with K_d values of ~1–2 μM. SD-36 binds to STAT2 and STAT5A with K_d values of ~5 μM and to STAT5B and STAT6 with weaker affinities (K_d > 10 μM). SD-36 therefore displays a high binding affinity to STAT3 and approximately 20-fold selectivity over STAT1 and STAT4.

We next investigated the selectivity of SD-36 in human peripheral blood mononuclear cells (PBMCs), which express all 7 STAT proteins. SD-36 potently and effectively reduced the levels of STAT3 protein in PBMCs (Figure 2E). Although SD-36 bound to STAT1 and STAT4 with good affinities (Figure S2E), it failed to degrade these two STAT proteins, as well as other STATs in PBMCs. SD-36 also potently and selectively induced the degradation of STAT3 without effect on other STATs in MOLM-16 and SU-DHL-1 cells (Figure 2A). Interestingly, STAT4 is transcriptionally upregulated upon SD-36 treatment in SU-DHL-1, but not in MOLM-16, PBMCs, or other cells tested (Figures 2A, 2E, and S2F). However, the phosphorylation of STAT4 at Tyr693 remained undetectable (Figure S2G), suggesting a lack of STAT4 activation.

To determine the proteome-wide selectivity of SD-36, we performed proteomic analyses in three cell lines. We tested SD-36 at 10 μM in an attempt to uncover any potential off-target effects. As shown in Figure 2F, of ~5,500 proteins quantified in each of these cell lines, STAT3 was the only protein whose level was significantly decreased by ≥2-fold ($p \leq 0.05$) by SD-36 at 10 μM. In comparison, the STAT3 inhibitor SI-109 at 10 μM had no measurable effect on the protein levels of STAT3 or other STATs (Figure S2H).

Taken together, these data show that SD-36 is a potent STAT3 degrader with exceptional selectivity over other STAT family members and >5,000 non-STAT proteins in cells.

SD-36 Effectively Degrades Mutated STAT3 Proteins in Cells

Somatic STAT3 mutations have been detected in several types of hematologic malignancies (Koskela et al., 2012; Pilati and Zucman-Rossi, 2015; Shahmarvand et al., 2018). A search of the Catalogue of Somatic Mutations in Cancer (Tate et al., 2019) revealed STAT3 mutations in 478 of 9,061 (5.3%) hematopoietic and lymphoid tumors, with most being hotspot mutations, such as D661Y, in the SH2 domain (Figure S2I).

Our co-crystal structure of SD-36 with STAT3 showed that D661 and K658 residues are not in direct contact with SD-36, suggesting that mutations at these residues may not affect the binding of SD-36 with STAT3. Indeed, SD-36 efficiently degrades endogenous D661Y and K658R mutant STAT3 proteins in cells (Figure 2G).

STAT3 is a latent transcription factor, and is activated upon phosphorylation of Tyr705. We found that SD-36 also effectively degrades CRISPR-mutated homozygous Y705F mutant STAT3 protein in DLD-1/STAT3$^{Y705F/Y705F}$ cells (Figure 2H), demonstrating that phosphorylation of Tyr705 is not required for SD-36-induced STAT3 degradation.

Hence, SD-36 effectively degrades both wild-type and mutated STAT3 proteins in cells, provided the mutations do not affect the interactions between SD-36 and the protein.

SD-36 Is Highly Potent and Specific in Suppressing the Transcriptional Activity of STAT3

STAT3 dimerization is mediated by the interaction between a p-Tyr705-containing peptide and the SH2 domain, which is essential for its DNA binding and subsequent transcriptional activity (Shuai et al., 1994). SD-36 at 1 μM completely depletes both monomeric and dimeric STAT3 protein within 5 h in MOLM-16 cells (Figure 3A). In contrast, SI-109 and SD-36Me diminish STAT3 dimers at ~10 μM. SD-36 at 1 μM abolishes the DNA binding activity of STAT3 in MOLM-16 and SU-DHL-1 (Figure 3B). SI-109 at 10 μM only modestly reduces the DNA binding activity of STAT3 in these cell lines.

In addition to forming homodimers, STAT3 also forms heterodimers with STAT1 and STAT5A/B proteins (Delgoffe and Vignali, 2013). We found that a small proportion of either cellular STAT1 or STAT5A/B is associated with STAT3 in MOLM-16 cells (Figure S3A), but SD-36 has no significant effect on the DNA binding activities of STAT1, STAT5A, or STAT5B (Figure S3B).

We then assessed the effect of SD-36 on the transcriptional activity of STAT3, using a STAT3-dependent luciferase reporter cell line (Figure 3C). After a 24-h treatment, the STAT3 inhibitors SI-108 and SI-109 and the STAT3 degrader control SD-36Me modestly reduced the transcriptional activity of STAT3 (IC_{50} ~10 μM). In comparison, SD-36 achieved an IC_{50} of 10 nM in suppressing the transcriptional activity of STAT3 (Figure 3C). Lenalidomide alone had no significant effect on STAT3 transcriptional activity. SI-109 plus lenalidomide at 1:1 molar ratio had similar activity to that of SI-109 alone. Furthermore, SD-36 had a minimal effect on the transcriptional activities of STAT1 or STAT5A/B in their corresponding STAT-dependent reporter cell lines (Figures S3C–S3F).

We next examined the effect of SD-36 on the expression of STAT3 transcriptional targets in cells. To capture the early-response genes upon STAT3 depletion, we treated MOLM-16 cells with SD-36 for 8 h for RNA sequencing (RNA-seq) analysis. We found that a total of 34 and 125 genes were up- or downregulated by ≥2-fold ($p \leq 0.05$), respectively, by SD-36 (Figure 3D). Among the most downregulated genes are known STAT3 targets such as *BCL3*, *HCK*, *HGF*, *JAK3*, *PIM1*, *SOCS3*, and *VEGFA*, all implicated in human cancers (Carpenter and Lo, 2014). Gene set enrichment analysis (GSEA) with the STAT3 targets gene set GSE21670 (Durant et al., 2010) affirmed a highly significant enrichment (Figure 3E), suggesting that STAT3 depletion by SD-36 leads to downregulation of STAT3 transcriptional targets in MOLM-16. qRT-PCR confirmed that a set of STAT3 target genes were indeed significantly downregulated by SD-36 as early as 8 h after exposure (Figure 3F).

Thus, selective and efficient degradation of STAT3 by SD-36 specifically diminishes the transcriptional activity of STAT3 and alters the expression of a group of genes including known STAT3 target genes.

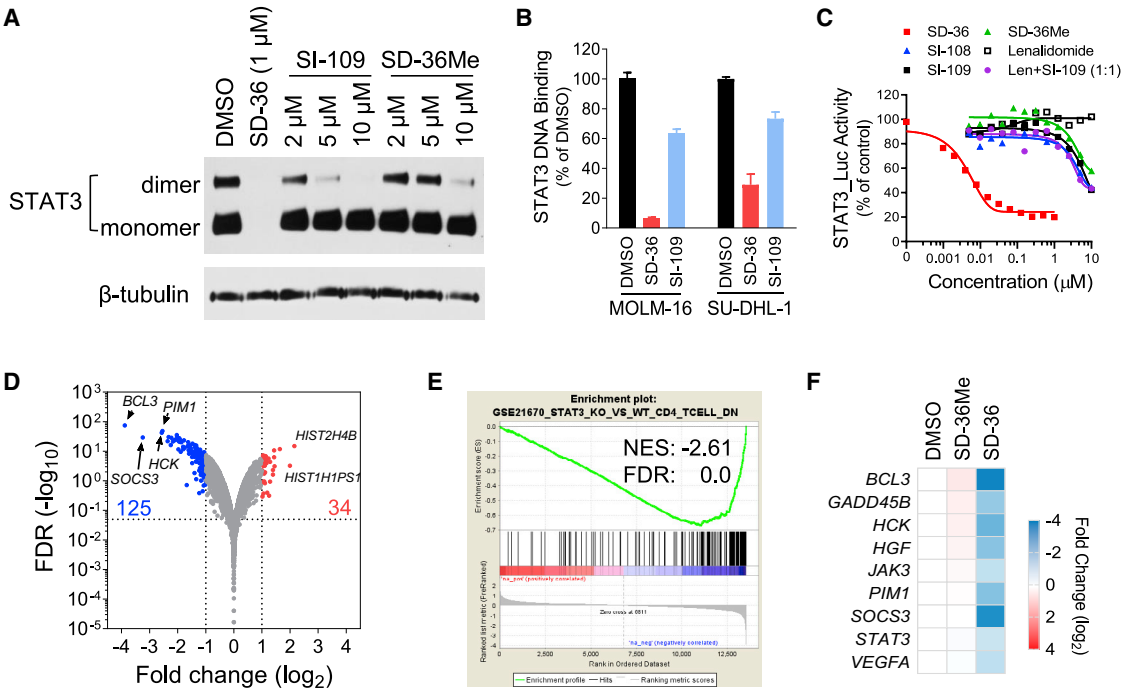

Figure 3. Effect of SD-36 on the Transcriptional Activity of STAT3

(A) MOLM-16 cells were treated for 5 h. Whole-cell lysis was subjected to native electrophoresis followed by immunoblotting.

(B) Cells were treated with 1 μM of SD-36 or 10 μM of SI-109 for 8 h. Nuclear extracts were prepared for STAT3 DNA binding activity assay (mean ± SEM; n = 3).

(C) MOLM-16 cells expressing STAT3-driven firefly luciferase gene were treated for 24 h for luciferase reporter assay. Representative concentration-response curves are shown.

(D) MOLM-16 cells were treated with 1 μM of SD-36 for 8 h for RNA-seq analysis. The horizontal dashed line marks the statistical significance (FDR $\leq$ 0.05) and the vertical lines mark the fold change (FC) ($|\log_2 FC| \geq 1$). Black arrows indicate representative genes validated by qRT-PCR. The numbers indicate genes that meet these criteria: blue, downregulated; red, upregulated. FDR, false discovery rate.

(E) GSEA showed the STAT3 targets gene set (GSE21670) is downregulated by SD-36 in MOLM-16 cells. NES, normalized enrichment score.

(F) MOLM-16 cells were treated with 1 μM of SD-36 or SD-36Me for 8 h for qRT-PCR. Data are the means of two independent experiments.

See also Figure S3.

SD-36 Displays Strong Growth Inhibitory Activities in a Subset of Leukemia and Lymphoma Cell Lines

We next evaluated STAT3 inhibitor SI-109 and degrader SD-36 for their cell growth inhibitory activities in human cancer cell lines.

Our initial testing revealed that STAT3 inhibitor SI-109 had no appreciable growth inhibitory activity in a large number of human cancer cell lines. Because STAT3 is frequently activated in leukemia and lymphoma (Arora et al., 2018; Bar-Natan et al., 2012), it is conceivable that these high-pSTAT3 (Y705) cell lines are more strongly dependent on STAT3 signaling for survival, and that degradation of STAT3 protein by SD-36 may achieve strong growth inhibitory activity. Thus, we evaluated SD-36 and its corresponding STAT3 inhibitor SI-109 in a panel of nine leukemia and nine lymphoma cell lines.

We found that SI-109 exerted a moderate growth inhibitory activity in only 1 of these 18 cell lines, MOLM-16 (IC_{50} ~3 μM), which has high level of pSTAT3 (Y705) (Figures 4A and 4B). In comparison, while SD-36 exhibited strong growth inhibitory activity in only one of nine AML cell lines, it demonstrated potent activity in five of nine lymphoma cell lines (Figure 4B). SD-36 achieved an IC_{50} of 35 nM in the MOLM-16 cell line and was nearly 100-fold more potent than SI-109. Of note, the SD-36-insensitive cell lines contain the components of Cul4A-CRBN E3 ligase complex (Figure S4A). In fact, SD-36 also effectively depleted cellular STAT3 protein in these cell lines (Figure S4B). Lenalidomide alone had only a modest effect on the proliferation of MOLM-16 (IC_{50} ~4 μM) and had no effect (IC_{50} > 10 μM) on the other cell lines tested (Figure 4C, data not shown). The combination of SI-109 with lenalidomide had an effect similar to that of SI-109 alone in MOLM-16 cells (Figure 4C).

Immunoblotting showed that SD-36 effectively depleted STAT3 protein and reduced the expression of c-Myc (Figure 4D), an important mediator of STAT3 oncogenic signaling (Bowman et al., 2001; Carpenter and Lo, 2014; Kiuchi et al., 1999). Although lenalidomide effectively depletes IKZF1, IKZF3, and CK1α, the neo-substrates of CRBN, upon the binding of immunomodulatory drugs to CRBN (Kronke et al., 2015; Lu et al., 2014), SD-36 had a very modest effect on the levels of these proteins (Figure 4D). The protein levels of GSPT1, a neo-substrate of CRBN modulator CC-885 (Matyskiela et al., 2016) and a potential off-target of CRBN-based PROTACs (Ishoey et al., 2018), was not affected by either SD-36 or lenalidomide (Figure 4D). Notably, SI-109 was ineffective in inhibition of STAT3 Y705 phosphorylation and in suppression of c-Myc expression at concentrations as high as 10 μM.

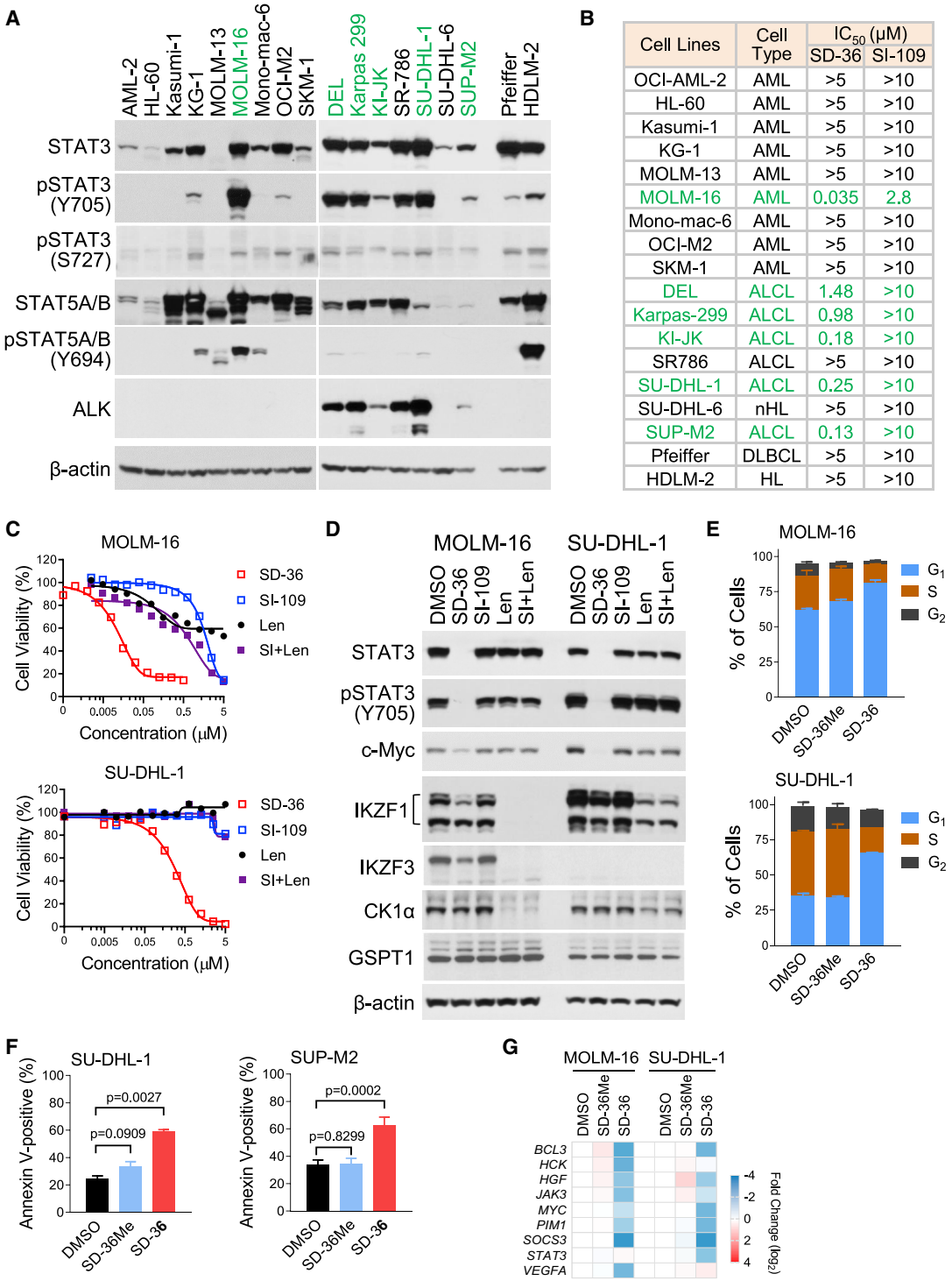

Cell Lines	Cell Type	IC_{50} (μM) SD-36	IC_{50} (μM) SI-109
OCI-AML-2	AML	>5	>10
HL-60	AML	>5	>10
Kasumi-1	AML	>5	>10
KG-1	AML	>5	>10
MOLM-13	AML	>5	>10
MOLM-16	AML	0.035	2.8
Mono-mac-6	AML	>5	>10
OCI-M2	AML	>5	>10
SKM-1	AML	>5	>10
DEL	ALCL	1.48	>10
Karpas-299	ALCL	0.98	>10
KI-JK	ALCL	0.18	>10
SR786	ALCL	>5	>10
SU-DHL-1	ALCL	0.25	>10
SU-DHL-6	nHL	>5	>10
SUP-M2	ALCL	0.13	>10
Pfeiffer	DLBCL	>5	>10
HDLM-2	HL	>5	>10

Figure 4. Growth Inhibitory Activity of SD-36 in AML and ALCL Cell Lines

(A) The expression of the indicated proteins was profiled by immunoblotting. SD-36-sensitive cell lines ($IC_{50} \leq 2$ μM) are labeled in green.

(B) The growth inhibitory activities of SD-36 and SI-109 in leukemia and lymphoma cell lines were determined by a 4-day CellTiter-Glo assay. IC_{50} values are the means of three independent experiments. DLBCL, diffuse large B cell lymphoma; HL, Hodgkin's lymphoma; nHL, non-Hodgkin's lymphoma. SD-36-sensitive cell lines ($IC_{50} \leq 2$ μM) are labeled in green.

(C) Representative concentration-response curves of CellTiter-Glo assay. Len, lenalidomide; SI + Len, SI-109 plus lenalidomide at 1:1 molar ratio.

(legend continued on next page)

To investigate the mode of growth inhibition mediated by SD-36, we examined its effect on cell cycles and apoptosis by flow cytometry. Treatment with SD-36 led to profound G_1 arrest and reduction of S phase cells in both MOLM-16 and SU-DHL-1 cell lines (Figure 4E). In comparison, SD-36Me only induced a modest G_1 arrest in MOLM-16 cells. Treatment with SD-36 also caused strong apoptotic cell death in SU-DHL-1 and SUP-M2 cells (Figure 4F). Immunoblotting confirmed the selective degradation of STAT3 by SD-36 in these cells (Figures S4C and S4D).

To gain insight into the potential mechanisms of SD-36-induced cell-cycle arrest and apoptosis, MOLM-16 and SU-DHL-1 cells were treated with SD-36 for 24 h then subjected to RNA-seq analysis. In MOLM-16, a total of 348 genes were up- or downregulated $\geq$2-fold ($p \leq 0.05$) by SD-36, with 47 upregulated and 301 downregulated. In comparison, only 13 genes were differentially regulated ($\geq$2-fold, $p \leq 0.05$) by SD-36Me after 24 h. GSEA revealed an overall marked decrease of the cytokine signaling following STAT3 degradation by SD-36 in MOLM-16 cells (false discovery rate < 0.01, Table S1). Genes typifying the reduced cytokine signaling include *BCL3* and *JAK3*, which were significantly downregulated by SD-36 (Figure 4G).

In SU-DHL-1, 726 and 701 genes were up- or downregulated by $\geq$2-fold ($p \leq 0.05$) by SD-36 at 24 h, respectively. In comparison, only 28 genes were differentially regulated ($\geq$2-fold, $p \leq 0.05$) by SD-36Me at 24 h. GSEA revealed downregulation of targets of c-Myc (Table S1), which plays a critical role in the pathogenesis and progression of a variety of cancers including ALCL (Dang, 2012; Gabay et al., 2014), but remains "undruggable" (Dang et al., 2017; McKeown and Bradner, 2014). To further evaluate the significance of c-Myc downregulation in SD-36 action, we transduced SU-DHL-1 cells with a lentiviral vector expressing c-Myc (Figure S4E). Overexpression of c-Myc significantly attenuated SD-36-mediated growth inhibition in SU-DHL-1 cells, albeit it had a modest effect on SD-36-induced apoptosis as assessed by caspase-3/7 activation and PARP cleavage (Figures S4E–S4G). These data demonstrate that downregulation of c-Myc contributes to SD-36-mediated growth inhibition in SU-DHL-1 cells.

In addition to its canonical function as a nuclear transcription factor upon Tyr705 phosphorylation, STAT3 has non-canonical functions, most notably in mitochondria (Srivastava and DiGiovanni, 2016). Mitochondrial STAT3 has been shown to regulate mitochondrial oxidative respiration directly in somatic cells (Gough et al., 2009; Wegrzyn et al., 2009) and indirectly in embryonic stem cells (Carbognin et al., 2016). Phosphorylation of STAT3 at Ser727 is critical for its mitochondrial translocation and function (Meier and Larner, 2014; Shulga and Pastorino, 2012; Tammineni et al., 2013; Wegrzyn et al., 2009). Wegrzyn et al. (2009) have shown that the activities of complexes I and II are diminished in *Stat3*-null mouse pro-B lymphocytes. Thus, we evaluated the effect of mitochondrial STAT3 degradation on the oxidative phosphorylation activities of complexes I and II. We found that while SD-36 effectively depleted mitochondrial STAT3 (Figure S4H), it did not have a substantial effect on complex I (Figure S4I) and II (Figure S4J). Our data are in line with recent studies that suggest that the role of mitochondrial STAT3 in oxidative phosphorylation depends on cellular context (Camporeale et al., 2014; Carbognin et al., 2016; Sala et al., 2019) and physiological conditions (Szczepanek et al., 2011). Given the many facets of STAT3 signaling, additional comprehensive investigations are warranted to assess the biological consequences of STAT3 depletion by SD-36 in tumor as well as normal tissues.

Collectively, selective degradation of SD-36 results in robust growth inhibition in a subset of leukemia and lymphoma cell lines. RNA-seq analysis reveals that STAT3 degrader SD-36 has more profound effect on downstream gene expression than STAT3 inhibitor SI-109.

SD-36 Effectively and Selectively Depletes STAT3 Protein in Mouse Xenograft Tumors

We next evaluated the therapeutic potential of SD-36 using mouse xenograft tumor models. Pharmacokinetics (PK) analysis showed that a single intravenous (i.v.) dose of SD-36 at 25 mg/kg in severe combined immunodeficiency (SCID) female mice achieved good drug exposure in plasma, tumor tissues, and several organs at 1, 3, and 6 h (Tables S2–S4). Pharmacodynamics (PD) analysis demonstrated that a single i.v. dose of SD-36 at 25 mg/kg depleted STAT3 protein by >80% at 1 h and >95% at 6 h and 24 h in MOLM-16 tumors (Figure 5A). The levels of STAT3 protein remained at <50% of controls in MOLM-16 tumors even 4 days after a single dose of SD-36 (Figure 5B). In comparison, SI-109 or SD-36Me at 100 mg/kg had no significant effect on the protein levels of STAT3 in MOLM-16 tumors (Figure 5C). A near-complete depletion of STAT3 protein was also achieved at 6 h and persisted for >24 h in both MOLM-16 and SU-DHL-1 tumors treated with a single dose of SD-36 (Figures 5A and S5A).

We next used multiplexed quantitative proteomics to evaluate the specificity of SD-36 in xenograft tumors. Consistent with its selective degradation of STAT3 in cultured cells *in vitro* (Figure 2F), SD-36 selectively depleted STAT3 protein but had no significant effect on other STAT proteins in MOLM-16 and SU-DHL-1 tumors *in vivo* (Figures 5D and S5B). qRT-PCR confirmed that a set of STAT3 target genes inhibited by SD-36 *in vitro* (Figure 3F) were significantly downregulated by a single dose of SD-36 *in vivo* (Figure 5E).

Collectively, SD-36 selectively degrades STAT3 *in vivo* and a single dose of SD-36 achieves a long-lasting PD effect in inducing STAT3 degradation in mouse xenograft tumors.

SD-36 Achieves Complete and Long-Lasting Tumor Regression in Mice

Based upon its strong PD effect in tumors, we evaluated SD-36 for its *in vivo* anti-tumor activity.

(D) Cells were treated with SD-36 (0.5 μM), SI-109 (1 μM), lenalidomide (Len) (1 μM), and SI-109 plus Len (1:1 molar ratio at 1 μM) for 24 h for immunoblotting.
(E) Cells were treated with 1 μM of SD-36 or SD-36Me for 48 h for cell-cycle analysis (mean ± SEM; n = 3).
(F) Cells treated for 48 h for apoptosis analysis by Annexin V staining (mean ± SEM; n = 3). p value, Student's t test.
(G) Cells were treated with 1 μM of SD-36Me or SD-36 for 24 h for qRT-PCR. Data are means of two independent experiments.
See also Figure S4 and Table S1.

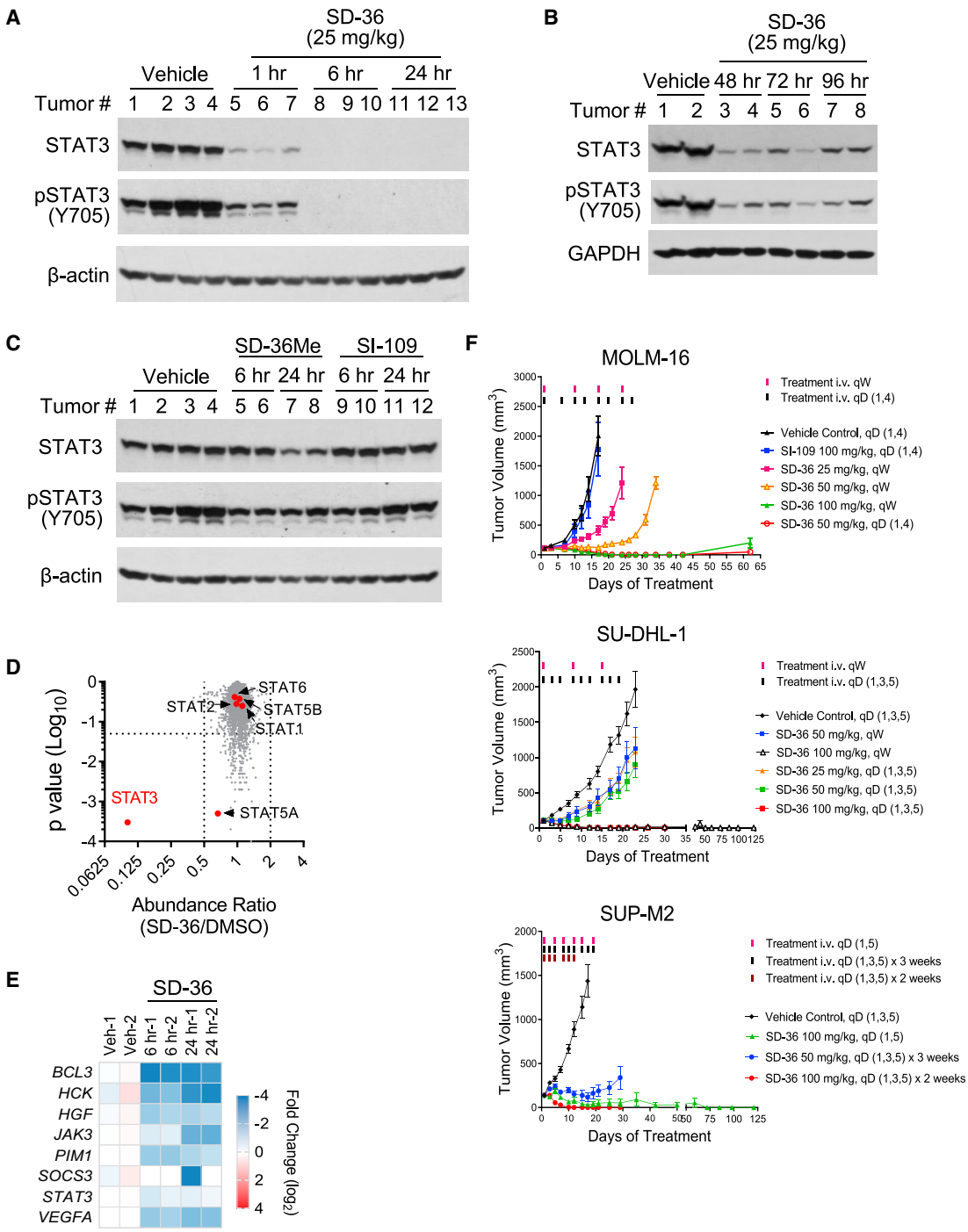

Figure 5. Anti-tumor Activity of SD-36 in Xenograft Tumor Models

(A) SCID mice bearing MOLM-16 tumors were treated i.v. as indicated. Tumor lysates were analyzed by immunoblotting.

(B) MOLM-16 tumors were analyzed by immunoblotting.

(C) SCID mice bearing MOLM-16 tumors were treated i.v. with 100 mg/kg of SD-36Me or SI-109. Tumor lysates were analyzed by immunoblotting.

(D) SCID mice bearing MOLM-16 tumors were treated with 25 mg/kg of SD-36 i.v. for 6 h. Tumor lysates were analyzed by multiplexed proteomics analysis. p value, Student's t test.

(E) SCID mice bearing MOLM-16 tumors were treated with vehicle control (veh) or 25 mg/kg of SD-36 i.v. Total RNAs were isolated from tumor lysates for qRT-PCR.

(F) Tumor-bearing SCID mice were treated at the indicated dosing schedules, and tumor volumes were measured every 2–3 days (mean ± SEM; n = 6–8). qD, daily; qW, weekly.

See also Figure S5.

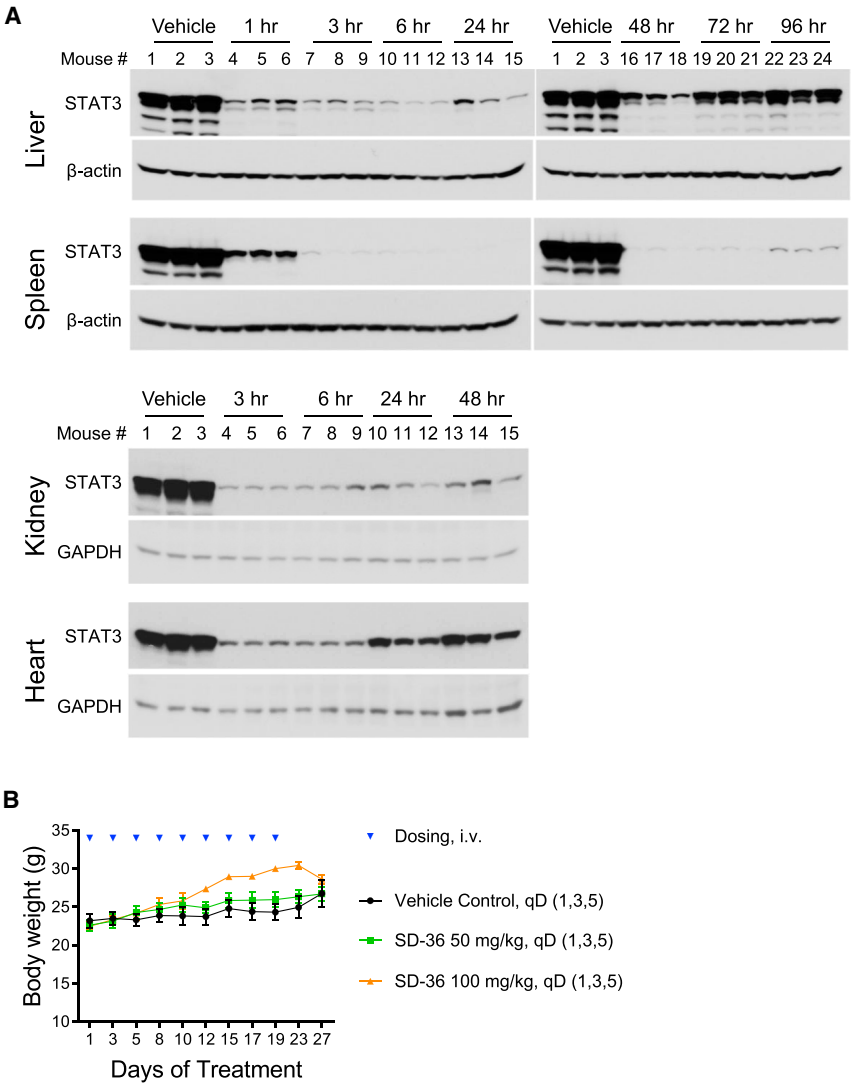

Figure 6. Toxicity of SD-36 in Immunocompetent Mice

(A) Female CD-1 mice were treated with SD-36 at 100 mg/kg i.v. Mouse tissues were analyzed by immunoblotting.

(B) CD-1 mice were treated i.v. for 3 weeks. Mouse body weight was measured every 2–3 days (mean ± SEM; n = 4–8). qD, daily.

See also Tables S2–S5 and Figure S6.

We first tested SD-36 in a MOLM-16 xenograft model in SCID female mice (Figure 5F, top). Because a single i.v. dose of SD-36 was capable of reducing the STAT3 protein level for >4 days, we evaluated the efficacy of SD-36 with infrequent dosing schedules in the MOLM-16 tumor model. We found that SD-36 at 25 and 50 mg/kg weekly dosing for 4 weeks effectively inhibited tumor growth. SD-36 at either 100 mg/kg weekly or 50 mg/kg twice weekly for 4 weeks induced complete tumor regression, which persisted for at least 2 weeks after cessation of treatment. In contrast, the STAT3 inhibitor SI-109 at 100 mg/kg twice weekly for 4 weeks had no effect on the growth of MOLM-16 tumors.

We further tested the efficacy of SD-36 in the SU-DHL-1 xenograft model (Figure. 5F, middle). In this model, SD-36 effectively inhibited tumor growth at 25 and 50 mg/kg administered on day 1, 3, and 5 per week and achieved complete tumor regression at 100 mg/kg with the same schedule. Although SD-36 at 50 mg/kg weekly inhibited tumor growth by 50% compared with the vehicle control, SD-36 at 100 mg/kg weekly achieved rapid and complete tumor regression. After a single dose of SD-36 at 100 mg/kg, tumor volume was reduced by 80% on day 6, and, after 2 doses, all tumors (7 out of 7) were completely regressed by day 12 with no tumor returning in 6 out of 7 mice on day 122, the end of the experiment and >100 days after the last dosing.

In the SUP-M2 tumor model, SD-36 at 50 mg/kg 3 times per week completely inhibited tumor growth (Figure 5F, lower). Complete tumor regression was achieved with dosing of SD-36 at 100 mg/kg 3 times per week, with the mice remaining tumor free until day 30, 15 days after the last dosing. SD-36 at 100 mg/kg twice a week for 3 weeks achieved complete tumor regression in 5 out of 7 tumors on day 29, with regressed tumors not growing back on day 121, the end of the experiment and >100 days after the last dosing.

In all these efficacy experiments, SD-36 caused no significant weight loss (Figure S5C) or other signs of toxicity.

Collectively, SD-36 is highly efficacious *in vivo* and is capable of achieving complete and long-lasting tumor regression in all the three xenograft models tested at well-tolerated dosing schedules.

SD-36 Induces Profound STAT3 Depletion in Mouse Tissues and Is Well Tolerated in Immune Competent Mice

Given the critical roles of STAT3 in multiple biological processes (Levy and Lee, 2002), we evaluated the potential toxicity of SD-36 in immune competent outbred CD-1 female mice.

We first performed PD analysis in four representative mouse tissues: liver, spleen, heart, and kidney. A single dose of SD-36 at 100 mg/kg causes a profound and durable depletion of mouse STAT3 protein in these tissues (Figure 6A).

To examine the potential toxicity, CD-1 mice were dosed with SD-36 i.v. at 50 and 100 mg/kg, 3 times a week for 3 weeks. Administration of SD-36 by these dosing regimens caused no obvious systemic toxicity as assessed by body weight and organ coefficient (including spleen, liver, kidney, and heart) (Figures 6B and S6A) and hematology analyses (Figure S6B). For example, no significant changes were observed in the counts of red or

white blood cells, lymphocytes, monocytes, or eosinophils in SD-36-treated versus control mice (Figure S6B). The numbers of neutrophils and platelets were slightly increased in SD-36 (100 mg/kg)-treated mice compared with the controls. SD-36 also had no significant effect on creatinine, blood urea nitrogen, calcium, albumin, and total blood protein (data not shown). Similarly, we observed no significant effects of pharmacologic degradation of STAT3 on the histology of mouse tissues examined (Figure S6C). In fact, SD-36-treated mice experienced moderate body weight gain (Figure 6B). This body weight gain was, however, reversible as SD-36-treated mice returned to the same body weight as vehicle control mice 1 week after SD-36 withdrawal (Figure 6B). Furthermore, SD-36-treated mice had comparable levels of blood glucose, bilirubin, alkaline phosphatase, and alanine aminotransferase with the vehicle control mice at the end of 3-week treatment (Figure S6D).

Altogether, SD-36 is well tolerated in immune competent CD-1 mice.

DISCUSSION

Dysregulation of STAT3 has been implicated in human cancers and other human diseases, and thus STAT3 has been intensely pursued as a therapeutic target. Unfortunately, targeting STAT3 with small molecules has proven to be very challenging for a number of reasons (Wong et al., 2017). Canonical STAT3 activation involves phosphorylation of its Tyr705 residue, which leads to STAT3 dimerization and subsequent nuclear translocation and transactivation of target genes. STAT3 dimerization mediated by pTyr705-SH2 domain interaction is critical for its DNA binding and subsequent transcriptional activity (Shuai et al., 1994). Therefore, extensive efforts have been devoted to the discovery and development of small-molecule inhibitors of the STAT3 SH2 domain. However, STAT3 dimerization also occurs in the absence of Tyr705 phosphorylation (Braunstein et al., 2003) and its nuclear translocation is independent of Tyr705 phosphorylation (Liu et al., 2005). Furthermore, unphosphorylated STAT3 also transcriptionally regulates the expression of a defined set of genes (Yang et al., 2005, 2007). Thus, blocking STAT3 dimerization with a small-molecule inhibitor is unlikely to completely block the transcriptional activity of STAT3. Second, because of the high sequence homology of the SH2 domain among STAT members, it is difficult to discover small molecules that bind to the STAT3 SH2 domain with high affinities and sufficient selectivity for unambiguous biological and pharmacological investigation of STAT3 as a therapeutic target. Our data show that, although SI-109 binds to STAT3 SH2 domain with a high affinity, it also displays good affinities to the SH2 domain of STAT1 and STAT4 proteins and achieves a selectivity of only ~20-fold. Such moderate selectivity is expected to be insufficient to provide unambiguous results with which STAT3 biology can be clearly defined *in vivo*. Although other approaches have been pursued for identification of small-molecule inhibitors of the STAT3 pathway, their mode of action and selectivity have yet to be clearly defined (Beebe et al., 2018). Hence, despite persistent research in the last 20 years, targeting STAT3 by a small-molecule inhibitor approach has not been successful.

PROTAC is an emerging technology for the development of a type of small-molecule therapy by inducing targeted protein degradation through hijacking the cellular protein degradation machinery. Therapeutically, there are at least two major advantages for PROTAC degraders over traditional small-molecule inhibitors of proteins. First, through efficient removal of a protein target by degradation, all the functions associated with the protein can be effectively blocked. Second, a PROTAC degrader can achieve much higher selectivity than the corresponding inhibitor since the degrader needs to bind to and recruit both the target protein and the E3 ligase to form a productive ternary complex for ubiquitination and degradation. Indeed, recent studies have shown that pan-BET bromodomain inhibitors, which bind to BRD2, BRD3, and BRD4 proteins with essentially the same affinities, can be used to successfully obtain selective BRD4 degraders (Chan et al., 2018; Gadd et al., 2017; Nowak et al., 2018; Zengerle et al., 2015).

In this study, we have developed SD-36 as a potent, selective, and efficacious PROTAC STAT3 degrader. While the corresponding STAT3 inhibitor SI-109 binds to STAT3 with a high affinity and has ~20-fold binding selectivity over STAT1 and STAT4, SD-36 degrades only STAT3 protein in cells and tumor tissues, demonstrating an exceptional selectivity among the STAT family proteins. Functionally, the degrader SD-36 is >1,000 times more potent than the inhibitor SI-109 in suppression of STAT3-dependent gene transcription. RNA-seq analysis demonstrates that degradation of STAT3 by SD-36 has much more profound effect on the downstream target genes of STAT3 than the STAT3 SH2 domain inhibitor SI-109 in tumor cells.

STAT3 is indispensable for early embryogenesis, and targeted disruption of *Stat3* in the mouse is embryonically lethal (Takeda et al., 1997). However, tissue-specific deletion of *Stat3* in adult mouse tissues exhibits non-lethal phenotypes (Levy and Lee, 2002). Concordantly, we found that systemic depletion of STAT3 protein by SD-36 in adult mice causes no overt toxicity. The main phenotype displayed by the STAT3-depleted CD-1 mice is reversible body weight gain. Previous studies in *Stat3* conditional knockout mice have demonstrated that STAT3 plays an essential role in glucose homeostasis and body weight regulation (Cernkovich et al., 2008; Cui et al., 2004; Inoue et al., 2004, 2006). The underlying mechanisms of mouse body weight gain upon acute STAT3 protein degradation warrants further investigation.

Our study has a number of important implications. First, it provides the very first example that the PROTAC technology can turn an essentially undruggable target such as STAT3 into a druggable target, thus paving the way for the design of PROTAC degraders for many other undruggable targets. Second, it provides another compelling example that the PROTAC technology can convert a modestly selective inhibitor into a protein degrader with extremely high selectivity. Third, our data demonstrate that a PROTAC degrader can achieve long-lasting downregulation of the target (>4 days) in tissues with only a single administration, making the clinical development of such a drug via i.v. administration feasible. Fourth, in contrast to the antisense oligonucleotide approach of targeting STAT3 (Hong et al., 2015), the PROTAC STAT3 degrader is capable of achieving complete tumor regression in multiple xenograft models, suggesting the potential superiority of STAT3 protein degradation over suppression of STAT3 mRNA expression as a therapeutic strategy.

In summary, we provide compelling data supporting SD-36 as a potent, selective, and highly efficacious PROTAC STAT3 degrader. Our study lays a solid foundation for the clinical development of a STAT3 degrader as a type of therapy for the treatment of human cancers and a number of other human diseases or conditions in which STAT3 plays a critical role.

STAR★METHODS

Detailed methods are provided in the online version of this paper and include the following:

- KEY RESOURCE TABLE
- LEAD CONTACT AND MATERIALS AVAILABILITY
- EXPERIMENTAL MODELS
  - Cell Lines
  - Mice
- METHOD DETAILS
  - Chemistry
  - Expression and Purification of STAT Proteins
  - Crystallization and Structure Determination of STAT3-SI109 and STAT3-SD36
  - Molecular Modeling
  - Fluorescence Polarization (FP) Assay
  - Biolayer Interferometry (BLI) Assay
  - Nuclear Extract Preparation and STAT DNA Binding Activity Assay
  - Site-Directed Mutagenesis of Human STAT3
  - Plasmid Purification and Transient Transfection
  - Silencing of *CRBN* Expression
  - Cell Viability Assay
  - Luciferase Reporter Assay
  - Cell Cycle and Annexin V Apoptosis Assays
  - Overexpression of c-Myc in SU-DHL-1 Cells
  - Caspase 3/7 Activity Assay
  - Mitochondrial OXPHOS Complex Enzyme Activity Assay
  - Co-immunoprecipitation (Co-IP)
  - Immunoblotting
  - Pervanadate (PV) Rreatment
  - Quantitative Reverse Rranscriptase-Polymerase Chain Reaction (qRT-PCR)
  - Transcriptomic Profiling
  - Proteomic Profiling
  - Statistical Analyses
- DATA AND CODE AVAILABILITY

SUPPLEMENTAL INFORMATION

Supplemental Information can be found online at https://doi.org/10.1016/j.ccell.2019.10.002.

ACKNOWLEDGMENTS

We are grateful for the financial support from Oncopia Therapeutics, Inc. (to S.W.) and for the Rogel Cancer Center Core grant (P30 CA046592) from the National Cancer Institute, NIH. This research used resources of the Advanced Photon Source, a U.S. Department of Energy (DOE) Office of Science User Facility operated for the DOE Office of Science by Argonne National Laboratory under contract no. DE-AC02-06CH11357. Use of the LS-CAT Sector 21 was supported by the Michigan Economic Development Corporation and the Michigan Technology Tri-Corridor (grant 085P1000817).

AUTHOR CONTRIBUTIONS

Conceptualization, L.B., H.Z., R.X., Y.Z., and S.W.; Methodology, L.B., H.Z., R.X., Y.Z., B.W., K.C., J.C., and J.L.M.; Investigation, L.B., H.Z., R.X., D.McE., C.-Y.Y., Z.L., M.W., L.L., B.W., P.K.; Formal Analysis, L.B., H. Z. D.McE., C.-Y.Y., Z.L., H.J., B.W., P. K., J.A.S., and S.W.; Resources, H.J., D.S., J.A.S., and S.W.; Writing – Original Draft, L.B, H.Z., J.A.S. and S.W.; Writing – Review & Editing, L.B, H.Z., Y.Z. and S.W.; Funding Acquisition, S.W.; Supervision, S.W.

DECLARATION OF INTERESTS

The University of Michigan has filed patent applications on SD-36 and its analogs, for which S.W., H.Z., R.X., L.B., D.McE., C.-Y.Y., and J.A.S. are co-inventors. These patents have been licensed by Oncopia Therapeutics, in which S.W. is a co-founder, a paid consultant, and owns stock. The University of Michigan also owns stock in Oncopia. This study is supported in part by a research contract from Oncopia.

Received: June 1, 2019
Revised: August 14, 2019
Accepted: October 7, 2019
Published: November 11, 2019

REFERENCES

Arora, L., Kumar, A.P., Arfuso, F., Chng, W.J., and Sethi, G. (2018). The role of signal transducer and activator of transcription 3 (STAT3) and its targeted inhibition in hematological malignancies. Cancers (Basel) *10*, https://doi.org/10.3390/cancers10090327.

Bai, L., Zhou, B., Yang, C.Y., Ji, J., McEachern, D., Przybranowski, S., Jiang, H., Hu, J., Xu, F., Zhao, Y., et al. (2017). Targeted degradation of BET proteins in triple-negative breast cancer. Cancer Res. *77*, 2476–2487.

Banerjee, K., and Resat, H. (2016). Constitutive activation of STAT3 in breast cancer cells: a review. Int. J. Cancer *138*, 2570–2578.

Bar-Natan, M., Nelson, E.A., Xiang, M., and Frank, D.A. (2012). STAT signaling in the pathogenesis and treatment of myeloid malignancies. JAKSTAT *1*, 55–64.

Becker, S., Groner, B., and Muller, C.W. (1998). Three-dimensional structure of the Stat3beta homodimer bound to DNA. Nature *394*, 145–151.

Beebe, J.D., Liu, J.Y., and Zhang, J.T. (2018). Two decades of research in discovery of anticancer drugs targeting STAT3, how close are we? Pharmacol. Ther. *191*, 74–91.

Bondeson, D.P., and Crews, C.M. (2017). Targeted protein degradation by small molecules. Annu. Rev. Pharmacol. Toxicol. *57*, 107–123.

Bondeson, D.P., Mares, A., Smith, I.E., Ko, E., Campos, S., Miah, A.H., Mulholland, K.E., Routly, N., Buckley, D.L., Gustafson, J.L., et al. (2015). Catalytic in vivo protein knockdown by small-molecule PROTACs. Nat. Chem. Biol. *11*, 611–617.

Bowman, T., Broome, M.A., Sinibaldi, D., Wharton, W., Pledger, W.J., Sedivy, J.M., Irby, R., Yeatman, T., Courtneidge, S.A., and Jove, R. (2001). Stat3-mediated Myc expression is required for Src transformation and PDGF-induced mitogenesis. Proc. Natl. Acad. Sci. U S A *98*, 7319–7324.

Braunstein, J., Brutsaert, S., Olson, R., and Schindler, C. (2003). STATs dimerize in the absence of phosphorylation. J. Biol. Chem. *278*, 34133–34140.

Bricogne, G., Blanc, E., Brandl, M., Flensburg, C., Keller, P., Paciorek, W., Roversi, P., Sharff, A., Smart, O.S., Vonrhein, C., and Womack, T.O. (2017). BUSTER, 2.10.3 (Global Phasing Ltd).

Burslem, G.M., Smith, B.E., Lai, A.C., Jaime-Figueroa, S., McQuaid, D.C., Bondeson, D.P., Toure, M., Dong, H., Qian, Y., Wang, J., et al. (2018a). The advantages of targeted protein degradation over inhibition: an RTK case study. Cell Chem. Biol. *25*, 67–77.e63.

Camporeale, A., Demaria, M., Monteleone, E., Giorgi, C., Wieckowski, M.R., Pinton, P., and Poli, V. (2014). STAT3 activities and energy metabolism: dangerous liaisons. Cancers (Basel) *6*, 1579–1596.

Carbognin, E., Betto, R.M., Soriano, M.E., Smith, A.G., and Martello, G. (2016). Stat3 promotes mitochondrial transcription and oxidative respiration during maintenance and induction of naive pluripotency. EMBO J. *35*, 618–634.

Carpenter, R.L., and Lo, H.W. (2014). STAT3 target genes relevant to human cancers. Cancers (Basel) *6*, 897–925.

CCG. (2018). Molecular Operating Environment (MOE) (Chemical Computing Group Inc.), www.chemcomp.com.

Cer, R.Z., Mudunuri, U., Stephens, R., and Lebeda, F.J. (2009). IC_{50}-to-K_i: a web-based tool for converting IC_{50} to K_i values for inhibitors of enzyme activity and ligand binding. Nucleic Acids Res. *37*, W441–W445.

Cernkovich, E.R., Deng, J., Bond, M.C., Combs, T.P., and Harp, J.B. (2008). Adipose-specific disruption of signal transducer and activator of transcription 3 increases body weight and adiposity. Endocrinology *149*, 1581–1590.

Chan, K.H., Zengerle, M., Testa, A., and Ciulli, A. (2018). Impact of target warhead and linkage vector on inducing protein degradation: comparison of bromodomain and extra-terminal (BET) degraders derived from triazolodiazepine (JQ1) and tetrahydroquinoline (I-BET726) BET inhibitor scaffolds. J. Med. Chem. *61*, 504–513.

Chen, J., Bai, L., Bernard, D., Nikolovska-Coleska, Z., Gomez, C., Zhang, J., Yi, H., and Wang, S. (2010a). Structure-based design of conformationally constrained, cell-permeable STAT3 inhibitors. ACS Med. Chem. Lett. *1*, 85–89.

Chen, V.B., Arendall, W.B., 3rd, Headd, J.J., Keedy, D.A., Immormino, R.M., Kapral, G.J., Murray, L.W., Richardson, J.S., and Richardson, D.C. (2010b). MolProbity: all-atom structure validation for macromolecular crystallography. Acta Crystallogr. D Biol. Crystallogr. *66*, 12–21.

Cui, Y., Huang, L., Elefteriou, F., Yang, G., Shelton, J.M., Giles, J.E., Oz, O.K., Pourbahrami, T., Lu, C.Y., Richardson, J.A., et al. (2004). Essential role of STAT3 in body weight and glucose homeostasis. Mol. Cell Biol. *24*, 258–269.

Dang, C.V. (2012). MYC on the path to cancer. Cell *149*, 22–35.

Dang, C.V., Reddy, E.P., Shokat, K.M., and Soucek, L. (2017). Drugging the 'undruggable' cancer targets. Nat. Rev. Cancer *17*, 502–508.

Delgoffe, G.M., and Vignali, D.A. (2013). STAT heterodimers in immunity: a mixed message or a unique signal? JAKSTAT *2*, e23060.

Durant, L., Watford, W.T., Ramos, H.L., Laurence, A., Vahedi, G., Wei, L., Takahashi, H., Sun, H.W., Kanno, Y., Powrie, F., and O'Shea, J.J. (2010). Diverse targets of the transcription factor STAT3 contribute to T cell pathogenicity and homeostasis. Immunity *32*, 605–615.

Emsley, P., Lohkamp, B., Scott, W.G., and Cowtan, K. (2010). Features and development of coot. Acta Crystallogr. D Biol. Crystallogr. *66*, 486–501.

Farnaby, W., Koegl, M., Roy, M.J., Whitworth, C., Diers, E., Trainor, N., Zollman, D., Steurer, S., Karolyi-Oezguer, J., Riedmueller, C., et al. (2019). BAF complex vulnerabilities in cancer demonstrated via structure-based PROTAC design. Nat. Chem. Biol. *15*, 672–680.

Fischer, E.S., Bohm, K., Lydeard, J.R., Yang, H., Stadler, M.B., Cavadini, S., Nagel, J., Serluca, F., Acker, V., Lingaraju, G.M., et al. (2014). Structure of the DDB1-CRBN E3 ubiquitin ligase in complex with thalidomide. Nature *512*, 49–53.

Gabay, M., Li, Y., and Felsher, D.W. (2014). MYC activation is a hallmark of cancer initiation and maintenance. Cold Spring Harb Perspect. Med. *4*, https://doi.org/10.1101/cshperspect.a014241.

Gadd, M.S., Testa, A., Lucas, X., Chan, K.H., Chen, W., Lamont, D.J., Zengerle, M., and Ciulli, A. (2017). Structural basis of PROTAC cooperative recognition for selective protein degradation. Nat. Chem. Biol. *13*, 514–521.

Gough, D.J., Corlett, A., Schlessinger, K., Wegrzyn, J., Larner, A.C., and Levy, D.E. (2009). Mitochondrial STAT3 supports Ras-dependent oncogenic transformation. Science *324*, 1713–1716.

Haque, S.J., Flati, V., Deb, A., and Williams, B.R. (1995). Roles of protein-tyrosine phosphatases in Stat1 alpha-mediated cell signaling. J. Biol. Chem. *270*, 25709–25714.

Haque, S.J., Wu, Q., Kammer, W., Friedrich, K., Smith, J.M., Kerr, I.M., Stark, G.R., and Williams, B.R. (1997). Receptor-associated constitutive protein tyrosine phosphatase activity controls the kinase function of JAK1. Proc. Natl. Acad. Sci. U S A *94*, 8563–8568.

Haura, E.B., Turkson, J., and Jove, R. (2005). Mechanisms of disease: insights into the emerging role of signal transducers and activators of transcription in cancer. Nat. Clin. Pract. Oncol. *2*, 315–324.

Hong, D., Kurzrock, R., Kim, Y., Woessner, R., Younes, A., Nemunaitis, J., Fowler, N., Zhou, T., Schmidt, J., Jo, M., et al. (2015). AZD9150, a next-generation antisense oligonucleotide inhibitor of STAT3 with early evidence of clinical activity in lymphoma and lung cancer. Sci. Transl Med. *7*, 314ra185.

Inoue, H., Ogawa, W., Asakawa, A., Okamoto, Y., Nishizawa, A., Matsumoto, M., Teshigawara, K., Matsuki, Y., Watanabe, E., Hiramatsu, R., et al. (2006). Role of hepatic STAT3 in brain-insulin action on hepatic glucose production. Cell Metab. *3*, 267–275.

Inoue, H., Ogawa, W., Ozaki, M., Haga, S., Matsumoto, M., Furukawa, K., Hashimoto, N., Kido, Y., Mori, T., Sakaue, H., et al. (2004). Role of STAT-3 in regulation of hepatic gluconeogenic genes and carbohydrate metabolism in vivo. Nat. Med. *10*, 168–174.

Ishoey, M., Chorn, S., Singh, N., Jaeger, M.G., Brand, M., Paulk, J., Bauer, S., Erb, M.A., Parapatics, K., Muller, A.C., et al. (2018). Translation termination factor GSPT1 is a phenotypically relevant off-target of heterobifunctional phthalimide degraders. ACS Chem. Biol. *13*, 553–560.

Johnson, D.E., O'Keefe, R.A., and Grandis, J.R. (2018). Targeting the IL-6/JAK/STAT3 signalling axis in cancer. Nat. Rev. Clin. Oncol. *15*, 234–248.

Jones, G., Willett, P., Glen, R.C., Leach, A.R., and Taylor, R. (1997). Development and validation of a genetic algorithm for flexible docking. J. Mol. Biol. *267*, 727–748.

Kiuchi, N., Nakajima, K., Ichiba, M., Fukada, T., Narimatsu, M., Mizuno, K., Hibi, M., and Hirano, T. (1999). STAT3 is required for the gp130-mediated full activation of the c-myc gene. J. Exp. Med. *189*, 63–73.

Koskela, H.L., Eldfors, S., Ellonen, P., van Adrichem, A.J., Kuusanmaki, H., Andersson, E.I., Lagstrom, S., Clemente, M.J., Olson, T., et al. (2012). Somatic STAT3 mutations in large granular lymphocytic leukemia. N. Engl. J. Med. *366*, 1905–1913.

Kronke, J., Fink, E.C., Hollenbach, P.W., MacBeth, K.J., Hurst, S.N., Udeshi, N.D., Chamberlain, P.P., Mani, D.R., Man, H.W., Gandhi, A.K., et al. (2015). Lenalidomide induces ubiquitination and degradation of CK1alpha in del(5q) MDS. Nature *523*, 183–188.

Lai, A.C., and Crews, C.M. (2017). Induced protein degradation: an emerging drug discovery paradigm. Nat. Rev. Drug Discov. *16*, 101–114.

Lee, H., Pal, S.K., Reckamp, K., Figlin, R.A., and Yu, H. (2011). STAT3: a target to enhance antitumor immune response. Curr. Top. Microbiol. Immunol. *344*, 41–59.

Levy, D.E., and Lee, C.K. (2002). What does Stat3 do? J. Clin. Invest. *109*, 1143–1148.

Liberzon, A., Birger, C., Thorvaldsdottir, H., Ghandi, M., Mesirov, J.P., and Tamayo, P. (2015). The Molecular Signatures Database (MSigDB) hallmark gene set collection. Cell Syst. *1*, 417–425.

Liberzon, A., Subramanian, A., Pinchback, R., Thorvaldsdottir, H., Tamayo, P., and Mesirov, J.P. (2011). Molecular signatures database (MSigDB) 3.0. Bioinformatics *27*, 1739–1740.

Liu, L., McBride, K.M., and Reich, N.C. (2005). STAT3 nuclear import is independent of tyrosine phosphorylation and mediated by importin-alpha3. Proc. Natl. Acad. Sci. U S A *102*, 8150–8155.

Lu, G., Middleton, R.E., Sun, H., Naniong, M., Ott, C.J., Mitsiades, C.S., Wong, K.K., Bradner, J.E., and Kaelin, W.G., Jr. (2014). The myeloma drug lenalidomide promotes the cereblon-dependent destruction of Ikaros proteins. Science *343*, 305–309.

Lu, J., Qian, Y., Altieri, M., Dong, H., Wang, J., Raina, K., Hines, J., Winkler, J.D., Crew, A.P., Coleman, K., and Crews, C.M. (2015). Hijacking the E3 ubiquitin ligase cereblon to efficiently target BRD4. Chem. Biol. *22*, 755–763.

Mandal, P.K., Limbrick, D., Coleman, D.R., Dyer, G.A., Ren, Z., Birtwistle, J.S., Xiong, C., Chen, X., Briggs, J.M., and McMurray, J.S. (2009). Conformationally

constrained peptidomimetic inhibitors of signal transducer and activator of transcription 3: evaluation and molecular modeling. J. Med. Chem. *52*, 2429–2442.

Mandal, P.K., Morlacchi, P., Knight, J.M., Link, T.M., Lee, G.R., Nurieva, R., Singh, D., Dhanik, A., Kavraki, L., Corry, D.B., et al. (2015). Targeting the Src homology 2 (SH2) domain of signal transducer and activator of transcription 6 (STAT6) with cell-permeable, phosphatase-stable phosphopeptide mimics potently inhibits Tyr641 phosphorylation and transcriptional activity. J. Med. Chem. *58*, 8970–8984.

Matyskiela, M.E., Lu, G., Ito, T., Pagarigan, B., Lu, C.C., Miller, K., Fang, W., Wang, N.Y., Nguyen, D., Houston, J., et al. (2016). A novel cereblon modulator recruits GSPT1 to the CRL4(CRBN) ubiquitin ligase. Nature *535*, 252–257.

McAlister, G.C., Nusinow, D.P., Jedrychowski, M.P., Wuhr, M., Huttlin, E.L., Erickson, B.K., Rad, R., Haas, W., and Gygi, S.P. (2014). MultiNotch MS3 enables accurate, sensitive, and multiplexed detection of differential expression across cancer cell line proteomes. Anal. Chem. *86*, 7150–7158.

McCoy, A.J., Grosse-Kunstleve, R.W., Adams, P.D., Winn, M.D., Storoni, L.C., and Read, R.J. (2007). Phaser crystallographic software. J. Appl. Crystallogr. *40*, 658–674.

McKeown, M.R., and Bradner, J.E. (2014). Therapeutic strategies to inhibit MYC. Cold Spring Harb Perspect. Med. *4*, https://doi.org/10.1101/cshperspect.a014266.

Meier, J.A., and Larner, A.C. (2014). Toward a new STATe: the role of STATs in mitochondrial function. Semin. Immunol. *26*, 20–28.

Neklesa, T.K., Winkler, J.D., and Crews, C.M. (2017). Targeted protein degradation by PROTACs. Pharmacol. Ther. *174*, 138–144.

Nowak, R.P., DeAngelo, S.L., Buckley, D., He, Z., Donovan, K.A., An, J., Safaee, N., Jedrychowski, M.P., Ponthier, C.M., Ishoey, M., et al. (2018). Plasticity in binding confers selectivity in ligand-induced protein degradation. Nat. Chem. Biol. *14*, 706–714.

Olson, C.M., Jiang, B., Erb, M.A., Liang, Y., Doctor, Z.M., Zhang, Z., Zhang, T., Kwiatkowski, N., Boukhali, M., Green, J.L., et al. (2018). Pharmacological perturbation of CDK9 using selective CDK9 inhibition or degradation. Nat. Chem. Biol. *14*, 163–170.

Otwinowski, Z., and Minor, W. (1997). Processing of X-ray diffraction data collected in oscillation mode. Methods Enzymol. *276*, 307–326.

Paiva, S.L., and Crews, C.M. (2019). Targeted protein degradation: elements of PROTAC design. Curr. Opin. Chem. Biol. *50*, 111–119.

Pettersson, M., and Crews, C.M. (2019). PROteolysis TArgeting Chimeras (PROTACs)—past, present and future. Drug Discov. Today Technol. *31*, 15–27.

Pilati, C., and Zucman-Rossi, J. (2015). Mutations leading to constitutive active gp130/JAK1/STAT3 pathway. Cytokine Growth Factor Rev. *26*, 499–506.

Reich, M., Liefeld, T., Gould, J., Lerner, J., Tamayo, P., and Mesirov, J.P. (2006). GenePattern 2.0. Nat. Genet. *38*, 500–501.

Sala, D., Cunningham, T.J., Stec, M.J., Etxaniz, U., Nicoletti, C., Dall'Agnese, A., Puri, P.L., Duester, G., Latella, L., and Sacco, A. (2019). The Stat3-Fam3a axis promotes muscle stem cell myogenic lineage progression by inducing mitochondrial respiration. Nat. Commun. *10*, 1796.

Schiedel, M., Herp, D., Hammelmann, S., Swyter, S., Lehotzky, A., Robaa, D., Olah, J., Ovadi, J., Sippl, W., and Jung, M. (2018). Chemically induced degradation of sirtuin 2 (Sirt2) by a proteolysis targeting chimera (PROTAC) based on sirtuin rearranging ligands (SirReals). J. Med. Chem. *61*, 482–491.

Shahmarvand, N., Nagy, A., Shahryari, J., and Ohgami, R.S. (2018). Mutations in the signal transducer and activator of transcription family of genes in cancer. Cancer Sci. *109*, 926–933.

Shuai, K., Horvath, C.M., Huang, L.H., Qureshi, S.A., Cowburn, D., and Darnell, J.E., Jr. (1994). Interferon activation of the transcription factor Stat91 involves dimerization through SH2-phosphotyrosyl peptide interactions. Cell *76*, 821–828.

Shulga, N., and Pastorino, J.G. (2012). GRIM-19-mediated translocation of STAT3 to mitochondria is necessary for TNF-induced necroptosis. J. Cell Sci. *125*, 2995–3003.

Smart, O.S., Womack, T.O., Sharff, A., Flensburg, C., Keller, P., Paciorek, W., Vonrhein, C., and Bricogne, G. (2017). GRADE, 1.2.13 (Global Phasing Ltd).

Smyth, M.S., Ford, H., and Burke, T.R. (1992). A general-method for the preparation of benzylic alpha,alpha-difluorophosphonic acids—nonhydrolyzable mimetics of phosphotyrosine. Tetrahedron Lett. *33*, 4137–4140.

Srivastava, J., and DiGiovanni, J. (2016). Non-canonical Stat3 signaling in cancer. Mol. Carcinog. *55*, 1889–1898.

Subramanian, A., Tamayo, P., Mootha, V.K., Mukherjee, S., Ebert, B.L., Gillette, M.A., Paulovich, A., Pomeroy, S.L., Golub, T.R., Lander, E.S., and Mesirov, J.P. (2005). Gene set enrichment analysis: a knowledge-based approach for interpreting genome-wide expression profiles. Proc. Natl. Acad. Sci. U S A *102*, 15545–15550.

Szczepanek, K., Chen, Q., Derecka, M., Salloum, F.N., Zhang, Q., Szelag, M., Cichy, J., Kukreja, R.C., Dulak, J., Lesnefsky, E.J., and Larner, A.C. (2011). Mitochondrial-targeted signal transducer and activator of transcription 3 (STAT3) protects against ischemia-induced changes in the electron transport chain and the generation of reactive oxygen species. J. Biol. Chem. *286*, 29610–29620.

Takeda, K., Noguchi, K., Shi, W., Tanaka, T., Matsumoto, M., Yoshida, N., Kishimoto, T., and Akira, S. (1997). Targeted disruption of the mouse Stat3 gene leads to early embryonic lethality. Proc. Natl. Acad. Sci. U S A *94*, 3801–3804.

Tammineni, P., Anugula, C., Mohammed, F., Anjaneyulu, M., Larner, A.C., and Sepuri, N.B. (2013). The import of the transcription factor STAT3 into mitochondria depends on GRIM-19, a component of the electron transport chain. J. Biol. Chem. *288*, 4723–4732.

Tate, J.G., Bamford, S., Jubb, H.C., Sondka, Z., Beare, D.M., Bindal, N., Boutselakis, H., Cole, C.G., Creatore, C., Dawson, E., et al. (2019). COSMIC: the catalogue of somatic mutations. Cancer Nucleic Acids Res. *47*, D941–D947.

Wegrzyn, J., Potla, R., Chwae, Y.J., Sepuri, N.B., Zhang, Q., Koeck, T., Derecka, M., Szczepanek, K., Szelag, M., Gornicka, A., et al. (2009). Function of mitochondrial Stat3 in cellular respiration. Science *323*, 793–797.

Winter, G.E., Mayer, A., Buckley, D.L., Erb, M.A., Roderick, J.E., Vittori, S., Reyes, J.M., di Iulio, J., Souza, A., Ott, C.J., et al. (2017). BET bromodomain proteins function as master transcription elongation factors independent of CDK9 recruitment. Mol. Cell *67*, 5–18.e19.

Wong, A.L.A., Hirpara, J.L., Pervaiz, S., Eu, J.Q., Sethi, G., and Goh, B.C. (2017). Do STAT3 inhibitors have potential in the future for cancer therapy? Expert Opin. Investig. Drugs *26*, 883–887.

Yang, J., Chatterjee-Kishore, M., Staugaitis, S.M., Nguyen, H., Schlessinger, K., Levy, D.E., and Stark, G.R. (2005). Novel roles of unphosphorylated STAT3 in oncogenesis and transcriptional regulation. Cancer Res. *65*, 939–947.

Yang, J., Liao, X., Agarwal, M.K., Barnes, L., Auron, P.E., and Stark, G.R. (2007). Unphosphorylated STAT3 accumulates in response to IL-6 and activates transcription by binding to NFkappaB. Genes Dev. *21*, 1396–1408.

Yang, J., and Stark, G.R. (2008). Roles of unphosphorylated STATs in signaling. Cell Res. *18*, 443–451.

Yu, H., and Jove, R. (2004). The STATs of cancer—new molecular targets come of age. Nat. Rev. Cancer *4*, 97–105.

Zengerle, M., Chan, K.H., and Ciulli, A. (2015). Selective small molecule induced degradation of the BET bromodomain protein BRD4. ACS Chem. Biol. *10*, 1770–1777.

Zhao, C., Li, H., Lin, H.J., Yang, S., Lin, J., and Liang, G. (2016). Feedback activation of STAT3 as a cancer drug-resistance mechanism. Trends Pharmacol. Sci. *37*, 47–61.

STAR★METHODS

KEY RESOURCE TABLE

REAGENT or RESOURCE	SOURCE	IDENTIFIER
Antibodies		
Stat1 Rabbit mAb	Cell Signaling Technology	Cat# 14994, RRID:AB_2737027
Phospho-STAT1 (Y701) Rabbit mAb	Cell Signaling Technology	Cat# 9167, RRID:AB_561284
Stat3 (D3Z2G) Rabbit mAb	Cell Signaling Technology	Cat# 12640, RRID:AB_2629499
Stat3 (79D7) (Sepharose® Bead Conjugate) Rabbit mAb	Cell Signaling Technology	Cat# 4368, RRID:AB_10692519
Phospho-Stat3 (Tyr705) (D3A7) XP Rabbit mAb	Cell Signaling Technology	Cat# 9145, RRID:AB_2491009
Phospho-Stat3 (Tyr705) (D3A7) XP® Rabbit mAb (HRP Conjugate) antibody	Cell Signaling Technology	Cat# 52075, RRID:AB_2799407
Phospho-Stat3 (Ser727) (D8C2Z) Rabbit mAb	Cell Signaling Technology	Cat# 94994, RRID:AB_2800239
STAT2 Rabbit mAb	Cell Signaling Technology	Cat# 72604, RRID:AB_2799824
STAT4 Rabbit mAb	Cell Signaling Technology	Cat# 2653, RRID:AB_2255156
Phospho-STAT4 (Y693) Rabbit mAb	Cell Signaling Technology	Cat#4134, RRID:AB_11179071
STAT5 Rabbit mAb	Cell Signaling Technology	Cat# 94205, RRID:AB_2737403
STAT5 Rabbit mAb	Cell Signaling Technology	Cat# 25656, RRID:AB_2798908
Phospho-STAT5 (Y694) Rabbit mAb	Cell Signaling Technology	Cat#4322, RRID:AB_10544692
Pim-1 Rabbit mAb	Cell Signaling Technology	Cat# 54523, RRID:AB_2799461
STAT6 Rabbit mAb	Cell Signaling Technology	Cat# 5397, RRID:AB_11220421
c-Myc Rabbit mAb	Cell Signaling Technology	Cat# 5605, RRID:AB_1903938
c-Myc Rabbit mAb	Cell Signaling Technology	Cat# 13987, RRID:AB_2631168
PARP Rabbit mAb	Cell Signaling Technology	Cat# 9532, RRID:AB_659884
CK1 (CK1α) Rabbit mAb	Cell Signaling Technology	Cat# 2655, RRID:AB_2283593
Ikaros (IKZF1) Rabbit mAb	Cell Signaling Technology	Cat# 14859, RRID:AB_2744523
Rabbit Anti-DYKDDDDK Tag Polyclonal Antibody, HRP Conjugated	Cell Signaling Technology	Cat# 2044, RRID:AB_10707327
Myc-Tag Rabbit mAb	Cell Signaling Technology	Cat#2278, RRID:AB_490778
β-Tubulin Rabbit polyclonal	Cell Signaling Technology	Cat#2146, RRID:AB_2210545
Mouse monoclonal ALK	Cell Signaling Technology	Cat#3791, RRID:AB_1950402
VDAC Rabbit mAb	Cell Signaling Technology	Cat#4661, RRID:AB_10557420
Ikaros (IKZF1) Rabbit mAb	Cell Signaling Technology	Cat# 14859, RRID:AB_2744523
Aiolos (IKZF3) Rabbit mAb	Cell Signaling Technology	Cat#15103, RRID:AB_2744524
CRBN Rabbit mAb	Cell Signaling Technology	Cat#71810, RRID:AB_2799810
CUL4A rabbit polyclonal	Cell Signaling Technology	Cat#2699, RRID:AB_2086563
DDB1 Rabbit mAb	Cell Signaling Technology	Cat#6998, RRID:AB_10829458
RBX1 Rabbit mAb	Cell Signaling Technology	Cat#11922, RRID:AB_2797769
CRBN rabbit polyclonal	Sigma-Aldrich	HPA045910, RRID:AB_10960409
CRBN rabbit polyclonal	Sigma-Aldrich	SAB2106014, RRID:AB_10744812
eRF3 (GSPT1) rabbit polyclonal	Abcam	ab126090, RRID:AB_11128263
c-Myc (9E10) mouse monoclonal	Santa Cruz Biotechnology	sc-40, RRID:AB_627268
GAPDH (0411) mouse monoclonal	Santa Cruz Biotechnology	Cat# sc-47724, RRID:AB_627678
Actin (C-2)	Santa Cruz Biotechnology	Cat# sc-8432, RRID:AB_626630
β-Actin Antibody (C4)	Santa Cruz Biotechnology	at# sc-47778 HRP, RRID:AB_2714189
Goat anti-Rabbit IgG (H+L) Secondary Antibody, HRP	Thermo Fisher Scientific	Cat#65-6120, RRID:AB_2533967
Goat anti-Mouse IgG (H+L) Secondary Antibody, HRP	Thermo Fisher Scientific	A28177, RRID:AB_2536163

(*Continued on next page*)

Continued

REAGENT or RESOURCE	SOURCE	IDENTIFIER
Bacterial and Virus Strains		
One Shot TOP10 Chemically Competent E. coli	Thermo Fisher Scientific	C404010
STAT3 Firefly luciferase reporter lentivirus (Puro)	Cellomics Technology	PLV-10065-50
LentiORF control particles	OriGene Technologies	PS100092V
Lenti ORF particles, MYC (Myc-DDK tagged)	OriGene Technologies	RC201611L1V
Lenti ORF particles, MYC (Myc-DDK tagged)	OriGene Technologies	RC201611L3V
SMARTvector Human Lentiviral CRBN shRNA	Dharmacon	V3SH7596-00EG51185
SMARTvector Empty Vector hCMV-TurboGFP Control Particles	Dharmacon	S-004000-01
Biological Samples		
Human PBMCs	ATCC	PCS-800-011
Human PBMCs	StemCell	#70025
Human PBMCs	IQ Biosciences	IQB-PBMC103
Chemicals, Peptides, and Recombinant Proteins		
SI-108	This study	NA
SI-109	This study	NA
SD-36	This study	NA
SD-36Me	This study	NA
SD-45FL	This study	NA
Lenalidomide	Sigma-Aldrich	Cat#901558, CAS#191732-72-6
Carfilzomib (PR-171)	Selleck Chemical	S2853, CAS# 868540-17-4
Pevonedistat (MLN4924)	Selleck Chemical	S7109, CAS# 905579-51-3
Sodium orthovanadate, Activated	Biovision	Cat#9471-5, CAS # 13721-39-6
Antimycin A	BioVision	Cat#2247-10, CAS # 1397-94-0
Rotenone	Abcam	ab143145, CAS# 83-79-4
2-Thenoyltrifluoroacetone	Cayman Chemical	Cat#15517, CAS# 326-91-0
Recombinant human IL-6 protein	Thermo Fisher Scientific	PHC0065
Recombinant mouse IL-3 protein	Thermo Fisher Scientific	PMC0034
Recombinant mouse IL-3 protein	R&D systems	403-ML
Recombinant human IFNγ	Sigma-Aldrich	I17001
STAT1 (132-713)	This study	NA
STAT2 (138-702)	This study	NA
STAT3 (127-688)	This study	NA
STAT4 (133-705)	This study	NA
STAT5A (136-705)	This study	NA
STAT5B (136-710)	This study	NA
STAT6 (113-658)	This study	NA
Critical Commercial Assays		
Ribo-Zero rRNA Removal Kit (Human/Mouse/Rat)	Illumina	MRZH11124
TruSeq mRNA Sample Prep v2 kit	Illumina	RS-122-2001
TruSeq mRNA Sample Prep v2 kit	Illumina	RS-122-2002
Mycoplasma Detection Kit	Lonza	LT07-318
QIAprep Spin Miniprep Kit	Qiagen	Cat#27106
RNeasy Mini Kit	Qiagen	Cat#74104
High-Capacity RNA-to-cDNA Kit	Thermo Fisher Scientific	Cat#4387406
TaqMan Fast Advanced Master Mix	Thermo Fisher Scientific	Cat#4444557
Power SYBR Green PCR Master Mix	Thermo Fisher Scientific	Cat#4368702
TMT10plex Isobaric Label Reagent	Thermo Fisher Scientific	Cat#90111

(*Continued on next page*)

Continued

REAGENT or RESOURCE	SOURCE	IDENTIFIER
EZ-Link Sulfo NHS-SS Biotinylation Kit	Thermo Fisher Scientific	Cat#21445
SuperSignal West Pico PLUS Chemiluminescent Substrate	Thermo Fisher Scientific	Cat#34580
Mitochondria Isolation Kit for Cultured Cells	Thermo Fisher Scientific	Cat#89874
TransAM STAT Family	Active Motif	Cat#42296
CellTiter-Glo Luminescent Cell Viability Assay	Promega	G7573
Luciferase Assay Reagent	Promega	E1483
Renilla Luciferase Assay System	Promega	E2810
Caspase-Glo 3/7 Assay	Promega	G8091
QuikChange II Site-Directed Mutagenesis Kit	Agilent Technologies	Cat#200524
Annexin-V-FLUOS Staining Kit	Sigma-Aldrich	Cat#11858777001
Complex I Enzyme Activity Microplate Assay Kit	Abcam	ab109721
Complex II Enzyme Activity Microplate Assay Kit	Abcam	ab109908
Bio-Rad Protein Assay	BIO-RAD	Cat#5000006
Deposited Data		
Raw RNA-seq data of MOLM-16 and SU-DHL-1	This study	GEO: GSE131358
Crystallography coordinates of SI-109-STAT3 complex	This study	PDB: 6NUQ
Crystallography coordinates of SD-36-STAT3 complex	This study	PDB: 6NJS
COSMIC	Tate et al., 2019	https://cancer.sanger.ac.uk/cosmic
Experimental Models: Cell Lines		
Human: MDA-MB-231	ATCC	HTB-26
Mouse: A20	ATCC	TIB-208
Human: OCI-AML2	DSMZ	ACC-99
Human: HL-60	DSMZ	ACC-3
Human: Kasumi-1	DSMZ	ACC-220
Human: KG-1	DSMZ	ACC-14
Human: MOLM-13	DSMZ	ACC-554
Human: MOLM-16	DSMZ	ACC-555
Human: MONO-MAC-6	DSMZ	ACC-124
Human: OCI-M2	DSMZ	ACC-619
Human: DEL	DSMZ	ACC-338
Human: SR-786	DSMZ	ACC-369
Human: SUP-M2	DSMZ	ACC-509
Human: SKM-1	DSMZ	ACC-547
Human: KI-JK	Japanese Cancer Research Resources Bank	JCRB1065
Mouse: Ba/F3/STAT5 Renilla luciferase reporter cell line	Crown Bioscience	NA
Human: Hela/Stat1 luciferase reporter cell line	Signosis	SL-0004-FP
Human: DLD-1	Horizon Discovery	HD 115-016
Human: DLD-1 (Y705F/Y705F)	Horizon Discovery	HD 115-016
Human: MOLM16/STAT3 luciferase reporter cell line	This study	NA
Experimental Models: Organisms/Strains		
Mouse: CB17/Icr-*Prkdc*^{scid}/IcrIcoCrl	Charles River Laboratories	Strain code: 236
Mouse: ICR (CD-1) Outbred Mice	Envigo	ICR (CD-1)
Oligonucleotides		
Primers for site-directed mutagenesis of STAT3 and SYBR RT-PCR, see Table S6	Custom-synthesized at the Thermo Fisher Scientific	N/A
GADD45B (Hs04188837_g1)	Thermo Fisher Scientific	Cat#4331182

(*Continued on next page*)

Continued

REAGENT or RESOURCE	SOURCE	IDENTIFIER
GAPDH (Hs02758991_g1)	Thermo Fisher Scientific	Cat#4331182
IL6 (Hs00985639_m1)	Thermo Fisher Scientific	Cat#4331182
MYC (Hs00153408_m1)	Thermo Fisher Scientific	Cat#4331182
Recombinant DNA		
pGL4[luc2P/STAT4-RE/Hygro] Vector	Promega	CS181501
pCMV6-Entry	OriGene Technologies	PS100001
pCMV6-STAT3-Myc-DDK	OriGene Technologies	RC215836
pCMV6-STAT3 (R609Q)-Myc-DDK	This study	NA
pCMV6-STAT3 (R609A)-Myc-DDK	This study	NA
pCMV6-STAT3 (R609E)-Myc-DDK	This study	NA
pCMV6-STAT3 (S611A/S613A)-Myc-DDK	This study	NA
Software and Algorithms		
GraphPad Prism 7	GraphPad	NA
MutationMapper	www.cbioportal.org/mutation_mapper	NA
R	www.r-project.org	NA
Amber 2018	http://ambermd.org/	NA
bcl2fastq v 2.17	Illumina	NA
GSEA	http://software.broadinstitute.org	NA
Bowtie v0.12.8	http://bowtie-bio.sourceforge.net	NA
GENCODE v24	www.gencodegenes.org	NA
Proteome Discoverer Software v2.1	Thermo Fisher Scientific	NA

LEAD CONTACT AND MATERIALS AVAILABILITY

Further information and requests for reagents may be directed to, and will be fulfilled by the corresponding author Shaomeng Wang at shaomeng@umich.edu.

EXPERIMENTAL MODELS

Cell Lines

MDA-MB-231, A20 and human PBMCs (PCS-800-011) were obtained from ATCC. OCI-AML2, HL-60, Kasumi-1, KG-1, MOLM-13, MOLM-16, MONO-MAC-6, OCI-M2, DEL, SR-786, SUP-M2 and SKM-1 were purchased from the DSMZ, the German Collection of Microorganisms and Cell Cultures GmbH. KI-JK was obtained from the Japanese Cancer Research Resources Bank. Ba/F3/STAT5 Renilla luciferase reporter cell line was from Crown Bioscience. Hela/Stat1 luciferase reporter was from the Signosis. Parental DLD-1 and DLD-1/STAT3$^{Y705F/Y705F}$ were from Horizon Discovery. Human PBMCs were also obtained from StemCell and IQ Biosciences. All the cells were cultured according to manufacturers' instructions. The established cell lines were used within 2 months after initiating from original stocks. PBMCs were recovered in RPMI-1640 medium supplemented with 10% Fetal Bovine Serum (Hyclone) for 2 days before treatment. To generate the MOLM-16/STAT3 luciferase reporter cell line, MOLM-16 cells were spinfected with STAT3 Firefly luciferase reporter lentivirus particles (Puro) (Cellomics Technology) at 2:1 cells/viral particles ratio in the presence of 8 μg/ml of polybrene (Sigma) for 1 hr at 500 × *g* and room temperature. Transduced cells were then transferred to fresh complete growth medium, and selected with 1 μg/mL puromycin (Invitrogen) 48 hr after transduction. About 2 weeks later, the puromycin-resistant MOLM/STAT3_Luc was used for reporter assay.

Mice

All the *in vivo* studies were performed under an animal protocol (PRO00007499) approved by the Institutional Animal Care & Use Committee of the University of Michigan, in accordance with the recommendations in the Guide for the Care and Use of Laboratory Animals of the National Institutes of Health.

For PK, PD and efficacy studies, SCID female mice were injected subcutaneously with 3 × 10^6 MOLM-16 cells, 1 × 10^7 SUP-M2 cells or 1 × 10^7 SU-DHL-1 cells in 5 mg/ml Matrigel (Corning) for tumor growth. When the tumors reached an average volume of

150 mm^3, mice were tumor size-matched and randomly assigned to different experimental groups for experiments. For PK and PD studies, mice were treated as described in the Results. At the indicated time-points, mice were euthanized and blood and tissue samples were collected for analyses. The PK analysis was performed by the University of Michigan Pharmacokinetics Core.

For toxicity studies in CD-1 female mice, mice were treated with SD-36 or vehicle control (10% PEG400 + 90% PBS) as described in the Results. Mouse body weights were measured 2-3 times per week. At the end of experiments, mice were euthanized and blood and main organs were collected for analyses. The toxicity studies, including hematology, chemistry and histology analyses, were performed by the University of Michigan Unit for Laboratory Animal Medicine *In Vivo* Animal Core.

For efficacy studies, drugs or vehicle control (10% PEG400 + 90% PBS) were given at the dose schedules as indicated in the Figures. Tumor sizes and animal weights were measured 2-3 times per week. Tumor volume (mm^3) = (length×$width^2$)/2. Tumor growth inhibition (TGI) was calculated as TGI (%) = $(V_c-V_t)/(V_c-V_o) \times 100$, where V_c and V_t are the medians of the control and treated groups at the end of the study respectively, and V_o at the start.

METHOD DETAILS

Chemistry

General Information

Experiments involving moisture- and/or air-sensitive components were performed in oven-dried glassware. Commercial solvents and reagents were used without further purification with the exceptions that THF was freshly distilled from sodium wire.

Flash column chromatography was performed using silica gel (type H) from TM Chemicals, Inc. Silica gel columns were typically packed as slurry and equilibrated with hexane prior to use. Analytical thin layer chromatography (TLC) was performed using Merck 60 F254 precoated silica gel plate (0.2 mm thickness). Subsequent to elution, plates were visualized under UV radiation. Further visualization, if necessary, was aided by staining with basic solution of potassium permanganate or acidic solution of ceric molybdate, followed by heating on a hot plate. The final products were purified by preparative high-performance liquid chromatography (HPLC) with a Waters Sunfire C18 reverse-phase HPLC column (50 mm × 100 mm) using solvent A (0.1% of TFA in water) and solvent B (0.1% of TFA in CH_3CN) as eluents with a flow rate of 60 mL/min. Proton nuclear magnetic resonance (^{1}H NMR), carbon nuclear magnetic resonance (^{13}C NMR) and phosphorus nuclear magnetic resonance (^{31}P NMR) spectroscopy were performed on Bruker Advance 300/400 NMR spectrometers. Chemical shifts of ^{1}H NMR spectra are reported as δ in units of parts per million (ppm) downfield from $SiMe_4$ (δ 0.0) and relative to the signal of chloroform-*d* (δ = 7.264, singlet). Multiplicities were given as: s (singlet); d (doublet); t (triplet); q (quartet); dd (doublet of doublets); ddd (doublet of doublets of doublets); dt (doublet of triplets); m (multiplets),etc. The number of protons for a given resonance is indicated by nH. Coupling constants are reported as *J* values in Hz. Carbon nuclear magnetic resonance spectra (^{13}C NMR) are reported as δ in units of parts per million (ppm) downfield from $SiMe_4$ (δ 0.0) and relative to the signal of chloroform-*d* (δ = 77.23, triplet). MS analyses were carried out with a Thermo-Scientific LCQ Fleet mass spectrometer or a Waters ultra-performance liquid chromatography (UPLC)–mass spectrometer

Synthesis of 5-((di-tert-butoxyphosphoryl)oxy)-1H-indole-2-carboxylic acid **(11)**.

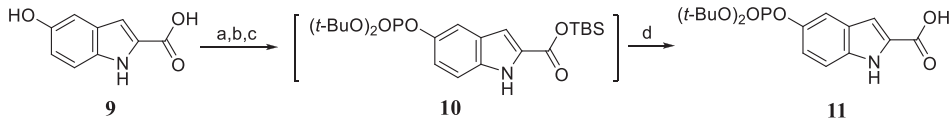

Reagents and conditions: a. TBSCl 1.4 equiv, *N*-Methylmorpholine; b. $(t\text{-BuO})_2$P-N(i-Pr)$_2$; c. t-BuO_2H; d. NH_4Cl sat. aqueous solution.

*5-((Di-tert-butoxyphosphoryl)oxy)-1H-indole-2-carboxylic acid (**11**).* Similar synthetic methods have been previously reported. (Mandal et al., 2009, 2015). To a round bottom flask equipped with a magnetic stirring bar was added **9** (1.0 mmol, 191 mg, 1.0 equiv.), TBS-Cl (150.7 mg, 1.0 mmol, 1.0 equiv.) and anhydrous THF (5 mL). To this solution, *N*-methylmorpholine (0.1 mL, 0.9 mmol, 0.9 equiv.) was added. After 1 hr, $(t\text{-BuO})_2$P-N(i-Pr)$_2$ (0.94 mL, 3.0 mmol, 3.0 equiv.) and tetrazole (0.45 N THF solution, 8.9 mL, 4.0 mmol, 4.0 equiv.) were added to the reaction mixture. The reaction mixture was allowed to stir 2 hr before addition of 70% t-BuO_2H (1.16 mL, 5.0 mmol) at 0°C. The mixture was further stirred for 6 rh before quenching with aqueous saturated solution of $Na_2S_2O_3$. The aqueous layer was extracted with ethyl acetate (3 × 30 mL) and the organic layers were combined and dried over anhydrous Na_2SO_4. The solvent was removed in vacuum and the product was recrystallized from ethyl acetate and hexane to give 0.27 g (68% yield) of **11**. ^{1}H NMR (300 MHz, MeOD-d_4): 8.95 (s, 1H), 7.49–7.38 (m, 2H), 7.16–7.06 (m, 2H), 1.35 (s, 18 H). ^{13}C NMR (75 MHz, MeOD-d_4): 146.7 (d, $J_{P\text{-}H}$ = 23.2 Hz), 146.4, 136.4, 129.1, 119.4 (d, $J_{P\text{-}H}$ = 4.19 Hz), 114.2, 113.2 (d, $J_{P\text{-}H}$ = 4.99 Hz), 109.3, 85.4 (d, $J_{P\text{-}H}$ = 7.85 Hz), 30.2 (d, $J_{P\text{-}H}$ = 4.39 Hz). ^{31}P NMR (121 MHz, MeOD-d_4): -15.2. ESI-MS calculated for $C_{17}H_{24}NO_6P$ $[M+Na]^+$ = 392.12, Found: 392.25.

*Synthesis of Compound **2**.*

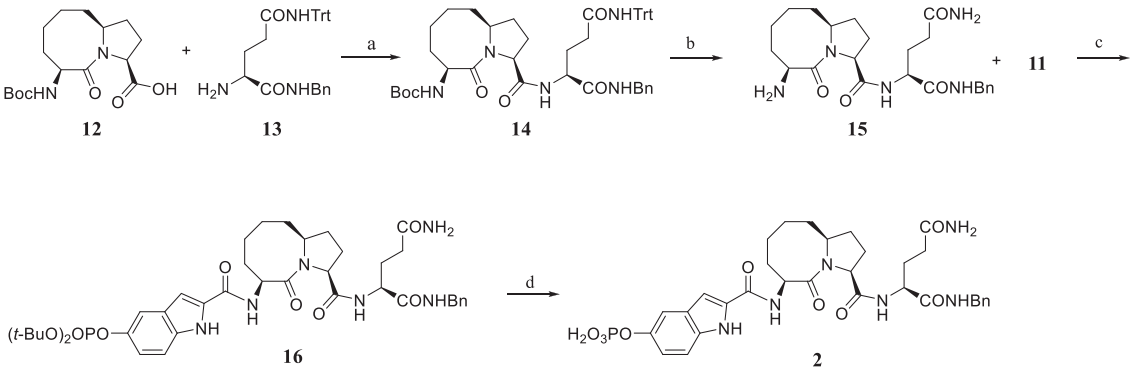

Reagents and conditions: a. EDC-HCl 2.0 equiv., HOBt 2.0 equiv., EtN(*i*-Pr)$_2$, CH_2Cl_2, room temperature (rt), 3 hr, 89% yield; b. CF_3CO_2H 2 mL, Et_3Si-H 0.1 mL, CH_2Cl_2 3 mL, rt, 1 hr; c. EDC-HCl, HOBt, EtN(*i*-Pr)$_2$, CH_2Cl_2, rt, 3 hr; d. TFA-CH_2Cl_2, rt, 3 hr.

*Tert-Butyl ((3S,6S,10aS)-3-(((S)-1-(benzylamino)-1,5-dioxo-5-(tritylamino)pentan-2-l)carbamoyl)-5-oxodecahydropyrrolo[1,2-a]azocin-6-yl)carbamate (**14**).* The known acid **12** (66 mg, 0.2 mmol), HOBt (56 mg, 0.4 mmol), and EDC-HCl (80 mg, 0.4 mmol) were placed in a round-bottom flask. EtN(iPr)$_2$ (0.2 mL, 1.0 mmol) and CH_2Cl_2 were added via syringes and the reaction mixture was stirred at room temperature for 5 min. **13** was added as a solution of CH_2Cl_2. The reaction was stirred at room temperature for 3 hr before quenching with saturated $NaHCO_3$. The aqueous layer was extracted with CH_2Cl_2 and the combined organic layers were washed with brine and dried over anhydrous sodium sulphate. The solvent was removed in vacuum and the residue was purified by flash column chromatography to yield **14** in 89% yield (0.14 g). ^{1}H NMR (300 MHz, MeOD-d4): 8.52 (s, 1H), 8.40-8.20 (m, 2H), 7.50-7.00 (m, 20 H), 4.70-4.45 (m, 1H), 4.45-4.20 (m, 5H), 2.70-2.40 (m, 2H), 2.30-1.00 (m, 14H), 1.44 (s, 9H). ^{13}C NMR (75 MHz, MeOD-d4): 174.60, 174.53, 173.96, 173.56, 157.57, 146.21, 139.92, 130.25, 129.69, 128.91, 128.68, 128.38, 127.93, 80.80, 71.74, 63.17, 61.63, 54.28, 52.14, 44.21, 37.46, 35.80, 33.60, 29.14, 28.95, 26.95, 23.53. ESI-MS calculated for $C_{47}H_{56}N_5O_6$ $[M+H]^+$ = 786.42, Obtained: 786.92.

*2-((3S,6S)-3-((S)-5-Amino-1-(benzylamino)-1,5-dioxopentan-2-ylcarbamoyl)-5-oxodecahydro-pyrrolo[1,2-a]azocin-6-ylcarbamoyl)-1H-indol-5-yl dihydrogen phosphate (**2**).* The amine **14** (78 mg, 0.1 mmol) was dissolved in CH_2Cl_2 (5 mL). Et_3Si-H (0.1 mL) and CF_3CO_2H (2 mL) were added via syringes. The reaction was stirred at room temperature for 1 hr. The volatile components were removed on a rotary evaporator. The obtained residue consisting of **15** was used for the next step without further purification. **15** (crude, 0.1 mmol) and **11** (55 mg, 0.15 mmol) were coupled using peptide coupling conditions (3.0 equiv HOBt. 3.0 equiv EDC-HCl, and 20 equiv. EtN(i-Pr)$_2$, CH_2Cl_2 as solvent). The product **16** was purified by flash column chromatography. In a round bottom flask equipped with a magnetic stirring bar, **16** was dissolved in CH_2Cl_2 (5 mL). CF_3CO_2H (2 mL) and Et_3Si-H (0.1 mL) were added to the reaction mixture, which was stirred for 3 hr. Solvent was removed by vacuum and the product was purified by reverse phase semi-preparative HPLC to give **2** (25 mg, 36% yield). ^{1}H NMR (300 MHz, MeOD-d4): 7.47 (s, 1H), 7.42 (d, *J* = 8.92 Hz, 1H), 7.38–7.20 (m, 5H), 7.17 (s, 1H), 7.13 (dd, *J* = 8.92, 1.67 Hz, 1H), 5.14–5.04 (m, 1H), 4.50–4.32 (m, 5H), 2.50–1.50 (m, 16H). ^{31}P NMR (121 MHz, MeOD-d4): 4.4 (s). ESI-MS calculated for $C_{32}H_{40}N_6O_9P$ $[M+H]^+$ = 683.26, Found: 683.20. Reverse phase analytical HPLC: > 99% purity.

*Synthesis of 3-((diethoxyphosphoryl)-difluoromethyl)-1H-indole-2-carboxylic acid **(24)**.*

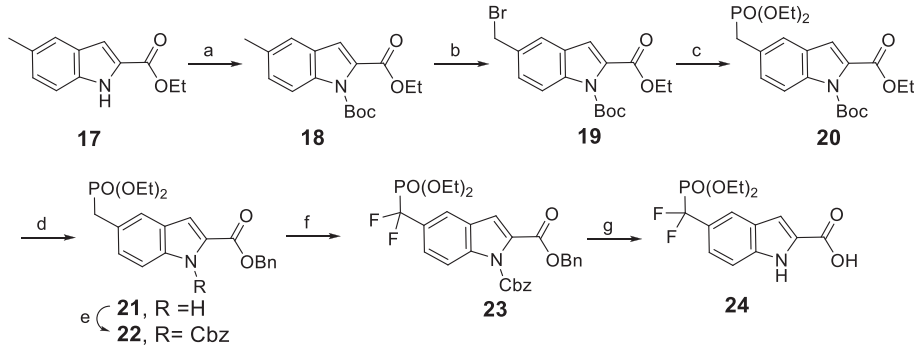

Reagents and conditions: a. NaH 2.0 equiv., Boc_2O 1.4 equiv., THF, 0°C to rt, 24 hr; b. NBS 1.0 equiv. Bz_2O_2 0.04 equiv. CCl_4, reflux 12 hr, 77% yield over two steps; c. $P(OEt)_3$ 1.2 equiv., 100°C, 12 hr, 84% yield; d. Ti(O-*i*-Pr)$_4$ 0.25 equiv. BnOH 20.0 equiv. 100°C, 83% yield; e. NaH 3.0 equiv. Cbz-Cl 1.5 equiv. THF, 0°C to rt, 12 hr, 88% yield; f. NFBS 3.0 equiv. NaHMDS 3.0 equiv., THF, -78°C to rt, 12 hr, 95% yield; g. H_2/Pd-C, THF, 12 hr, 94% yield.

1-Tert-Butyl 2-ethyl 5-(bromomethyl)-1H-indole-1,2-dicarboxylate ***(19)***. To a round bottom flask equipped with a magnetic stirring bar was added NaH (2.2 g, 53 mmol, 2.0 equiv., 60% in mineral oil) and THF (300 mL). The suspension was cooled with an ice/water bath before addition of ethyl 5-methyl-1*H*-indole-2-carboxylate **17** (5.0 g, 26 mmol, 1.0 equiv.) over 15 min. The solution was stirred at this temperature for 30 min (the colour of solution turned red). Boc_2O (8.1 g, 37 mmol, 1.4 equiv) was added to the solution in one portion. The reaction mixture was allowed to stir at room temperature for another 24 hr before quenching with ice water. The aqueous layer was extracted with ethyl acetate (200 mL × 2) and the combined organic layers were washed with brine (50 mL ×2), dried over anhydrous sodium sulphate, and concentrated on a rotary evaporator. The residual crude product **18** was used directly for the next step without further purification. To a round bottom flask equipped with a magnetic stirring bar was added previous crude **18**, $(PhCO)_2O_2$ (242 mg, 1.0 mmol, 0.04 equiv), NBS (4,62 g, 26.0 mmol, 1.0 equiv) and anhydrous CCl_4 (150 mL). The reaction mixture was heated at reflux for 12 hr. The precipitate was filtered off and the solvent was removed on a rotary evaporator. The residual crude product was purified by flash column chromatography to afford the desired benzylic bromide **19** as colourless oil (7.6 g, 77% yield). ^{1}H NMR (300 MHz, $CDCl_3$): 8.05 (d, J = 8.66 Hz, 1H), 7.61 9d, J = 1.39 Hz, 1H), 7.44 (dd, J = 8.66, 1.81 Hz, 1H), 7.06 (d, J = 0.65 Hz, 1H), 5.29 (s, 2H), 4.38 (q, J = 7.14 Hz, 2H), 1.62 (s, 9H), 1.40 (t, J = 7.14 Hz, 3H). ^{13}C NMR (75 MHz, $CDCl_3$): 161.8, 149.2, 146.9, 137.6, 133.0, 131.8, 128.0, 127.9, 122.7, 115.5, 114.5, 85.3, 85.0, 61.7, 34.1, 28.0, 14.4. ESI-MS calculated for $C_{17}H_{21}{}^{79}BrNO_4$ $[M+H]^+$ = 382.07, Found: 382.42; $C_{17}H_{21}{}^{81}BrNO_4$ $[M+H]^+$: 384.06, Found: 384.08.

1-Tert-Butyl 2-ethyl 5-((diethoxyphosphoryl)methyl)-1H-indole-1,2-dicarboxylate ***(20)***. To a round bottom flask equipped with a magnetic stirring bar was added **19** (3 g, 7.9 mmol, 1.0 equiv.) and $(EtO)_3P$ (1.72 mL, 10.0 mmol, 1.2 equiv.). The reaction mixture was heated at 100°C for 12 hr. The reaction mixture was loaded directly to silica gel column and purified by flash column chromatography to afford the desired phosphate **20** as a colourless oil (2.9 g, 84%). ^{1}H NMR (300 MHz, $CDCl_3$): 8.02 (d, J = 8.62 Hz, 1H), 7.53 (s, 1H), 7.35 (d, J = 8.63 Hz, 1H), 7.05 (s, 1H), 4.38 (q, J = 7.13 Hz, 2H), 4.07–3.92 (m, 4H), 3.23 (d, $J_{P\text{-}H}$ = 21.24 Hz, 2H), 1.63 (s, 9H), 1.39 (t, J = 7.13 Hz, 3H), 1.23 (t, J = 7.06 Hz, 6H). ^{13}C NMR (75 MHz, $CDCl_3$): 161.7, 149.1, 136.7 (d, $J_{P\text{-}C}$ = 2.88 Hz), 131.1, 128.5 (d, $J_{P\text{-}C}$ = 5.88 Hz), 127.7 (d, $J_{P\text{-}C}$ = 2.81), 126.5 (d, $J_{P\text{-}C}$ = 9.12 Hz), 122.9 (d, $J_{P\text{-}C}$ = 7.15 Hz), 114.8 (d, $J_{P\text{-}C}$ = 2.50 Hz), 114.3, 84.5, 62.0 (d, $J_{P\text{-}C}$ = 6.79 Hz), 61.3, 33.3 (d, $J_{P\text{-}C}$ = 128.4), 27.7, 16.3 (d, $J_{P\text{-}C}$ = 5.96 Hz), 14.1. ^{31}P NMR (121 MHz, $CDCl_3$): 26.3 (s). ESI-MS calculated for $C_{21}H_{31}NO_7P$ $[M+H]^+$ = 440.18, Found: 440.67.

Benzyl 5-((diethoxyphosphoryl)methyl)-1H-indole-2-carboxylate ***(21)***. To a round bottom flask equipped with a magnetic stirring bar was added **20** (2.9 g, 6.6 mmol, 1.0 equiv.), BnOH (14 mL, 132 mmol, 20 equiv.), and $Ti(O\textit{i}\text{-}Pr)_4$ (0.32 mL, 1.6 mmol, 0.25 equiv.). The reaction mixture was heated at 100°C for 12 hr. The reaction mixture was cooled down to 35°C and quenched with 1 *N* HCl (20 mL). The aqueous layer was extracted with ethyl acetate (200 mL × 2) and the combined organic extracts were washed with brine (50 mL ×2), dried over anhydrous sodium sulphate, filtered and concentrated in vacuum. The residual crude product was purified by flash column chromatography to afford the desired benzyl carboxylate **21** as a colourless oil (2.25 g, 83% yield). 80% purity (determined by ^{31}P NMR): 10% ethyl carboxylate, 10% unknown. ^{1}H NMR (300 MHz, MeOD-d4): 7.65 (s, 1H), 7.60–7.38 (m, 6H), 7.31 (dt, J = 8.57, 1.72 Hz, 1H), 7.24 (s, 1H), 5.43 (s, 2H), 4.15–4.00 (m, 4H), 3.35 (d, $J_{P\text{-}H}$ = 21.03 Hz, 2H), 1.30 (t, J = 7.06 Hz, 6H). ^{13}C NMR (75 MHz, MeOD-d4): 163.0, 138.2 (d, $J_{P\text{-}C}$ = 2.19 Hz), 137.6, 129.6, 129.3, 129.2, 129.1, 128.8 (d, $J_{P\text{-}C}$ = 2.76 Hz), 128.2 (d, $J_{P\text{-}C}$ = 5.33 Hz), 124.3 (d, $J_{P\text{-}C}$ = 7.95 Hz), 124.1 (d, $J_{P\text{-}C}$ = 9.42 Hz), 113.4 (d, $J_{P\text{-}C}$ = 2.37 Hz), 109.3, 67.4, 63.6 (d, $J_{P\text{-}C}$ = 6.96 Hz), 33.6 (d, $J_{P\text{-}C}$ = 138.3 Hz), 16.7 (d, $J_{P\text{-}C}$ = 5.92 Hz). ^{31}P NMR (121 M Hz, MeOD-d4): 28.3 (s), 26.4 (s). ESI-MS calculated for $C_{21}H_{25}NO_5P$ $[M+H]^+$ = 402.15, Found: 402.50.

Dibenzyl 5-((diethoxyphosphoryl)methyl)-1H-indole-1,2-dicarboxylate ***(22)***. To a round bottom flask equipped with a magnetic stirring bar was added NaH (0.6 g, 15 mmol, 3.0 equiv., 60% in mineral oil) and THF (100 mL). The suspension was cooled with ice/water bath before addition of **21** (2.25 g in THF, 5.5 mmol, 1.0 equiv.) over 5 min. The solution was stirred at this temperature for 10 min before addition of Cbz-Cl (1.12 mL, 8 mmol, 1.5 equiv.) via a syringe. The reaction mixture was stirred at room temperature for another 12 hr before quenching with ice water. The aqueous layer was extracted with ethyl acetate (200 mL × 2) and the combined organic extracts were washed with brine (50 mL ×2), dried over anhydrous sodium sulphate, and concentrated *in vacuum*. The residual crude product was purified by flash column chromatography to afford the desired **22** as colourless oil (2.6 g, 88% yield). ^{1}H NMR (300 MHz, $CDCl_3$): 8.00 (d, J = 8.63 Hz, 1H), 7.52 (s, 1H), 7.46–7.26 (m, 11H), 7.11 (s, 1H), 5.33 (s, 2H), 5.20 (s, 2H), 4.10–3.90 (m, 4H), 3.22 (d, $J_{P\text{-}H}$ = 21.30 Hz, 2H), 1.21 (t, J = 7.05 Hz, 6H). ^{13}C NMR (75 MHz, $CDCl_3$): 161.3, 150.5, 136.6 (d, $J_{P\text{-}C}$ = 2.97 Hz), 135.3, 134.4, 130.6, 129.0 (d, $J_{P\text{-}C}$ = 5.88 Hz) 128.7, 128.6, 128.6, 128.5, 128.3, 128.2, 127.8 (d, $J_{P\text{-}C}$ = 2.82 Hz), 127.0 (d, $J_{P\text{-}C}$ = 9.10 Hz), 123.1 (d, $J_{P\text{-}C}$ = 7.08 Hz), 115.6, 115.0 (d, $J_{P\text{-}C}$ = 2.25 Hz), 69.5, 67.1, 62.1 (d, $J_{P\text{-}C}$ = 6.78 Hz), 33.4 (d, $J_{P\text{-}C}$ = 138.49 Hz), 16.3 (d, $J_{P\text{-}C}$ = 5.87 Hz). ^{31}P NMR (121 M Hz, $CDCl_3$): 26.3 (s). ESI-MS calculated for $C_{29}H_{30}NO_7P$ $[M+Na]^+$ = 558.17, Found: 558.08.

Dibenzyl 5-((diethoxyphosphoryl)difluoromethyl)-1H-indole-1,2-dicarboxylate ***(23)***. To a round bottom flask equipped with a magnetic stirring bar was added **22** (9.17 g, 17 mmol, 1.0 equiv.), $(PhSO_2)_2NF$ (known as NFSB, 16 g, 51 mmol, 3.0 equiv.) and THF (300 mL). The reaction mixture was cooled to −78°C with the aid of an ethanol/dry ice bath. To this solution, NaHMDS (51 mL, 1.0 M in THF, 3.0 equiv.) was added over 10 min. The reaction mixture was allowed to stir at this temperature for 2 hr before warming up to room temperature over 3 to 4 hr. The reaction was quenched with saturated NH_4Cl aqueous solution (100 mL). The aqueous layer was extracted with ethyl acetate (200 mL × 2) and the combined organic extracts were washed with brine (50 mL × 2), dried over anhydrous sodium sulphate, and concentrated in vacuum. The residual crude product was purified by flash column chromatography to afford the desired product **23** as colourless oil (9.6 g, 95% yield). ^{1}H NMR (300 MHz, $CDCl_3$): 8.13 (d, J = 8.70 Hz, 1H), 7.88 (s, 1H), 7.65 (d, J = 8.90 Hz, 1H), 7.50–7.28 (m, 10H), 7.17 (s, 1H), 5.33 (s, 2H), 5.20 (s, 2H), 4.30–4.00

(m, 4H), 1.27 (t, J = 6.85 Hz, 6H). ^{13}C NMR (75 MHz, $CDCl_3$): 161.2, 150.3, 138.6, 135.2, 134.2, 131.5, 129.0, 128.8, 128.7, 128.6, 128.5, 128.4, 128.4–127.6 (m), 127.4, 125.2–124.4 (m), 121.0–120.6 (m), 120.5–119.5 (m), 115.5, 115.2, 70.0, 67.3, 64.9 (d, J_{P-C} = 6.76 Hz), 16.3 (d, J_{P-C} = 5.49 Hz). ^{31}P NMR (121 M Hz, $CDCl_3$): 6.3 (t, J_{P-F} = 117 Hz). ESI-MS calculated for $C_{29}H_{29}F_2NO_7P$ $[M+H]^+$ = 572.17, Found: 572.25.

*5-((Diethoxyphosphoryl)difluoromethyl)-1H-indole-2-carboxylic acid (**24**).* To a round bottom flask equipped with a magnetic stirring bar was added **23** (1 g, 1.7 mmol, 1.0 equiv.) and THF (300 mL). The oxygen was removed with the aid of a vacuum line and a nitrogen balloon. 10% Pd/C (0.1 g, 0.1 mmol, 0.05 equiv.) was added to the reaction mixture. The reaction was stirred at room temperature for 12 hr under H_2 atmosphere (1 atm H_2 balloon). The Pd/C was removed by filtration and the solvent was removed in vacuum. The residual crude product was purified by flash column chromatography to afford the desired **24** as a pale green solid (0.56 g, 94% yield). Higher purity can be achieved by recrystallization from $CHCl_3$. ^{1}H NMR (300 MHz, MeOD-d4): 11.6 (s, 1H), 7.94 (s, 1H), 7.58 (d, J = 8.75 Hz, 1H), 7.48 (d, J = 8.75 Hz, 1H), 7.27 (s, 1H), 4.30–4.05 (m, 4H), 1.30 (td, J = 7.04 Hz, J_{P-H} = 0.49 Hz, 6H). ^{13}C NMR (75 MHz, MeOD-d4): 164.5, 139.7, 131.2, 128.1, 126.0–124.0 (m), 123.4–123.0 (m), 122.4–122.0 (m), 119.0–118.1 (m), 113.5, 109.6, 66.3 (d, J_{P-C} = 7.09 Hz), 16.6 (d, J_{P-C} = 5.34 Hz). ^{31}P NMR (121 M Hz, MeOD-d4): 6.6 (t, J_{P-F} = 123 Hz). ESI-MS calculated for $C_{14}H_{17}F_2NO_5P$ $[M+H]^+$ = 348.08, Found: 348.42.

*Synthesis of Compound **3**.*

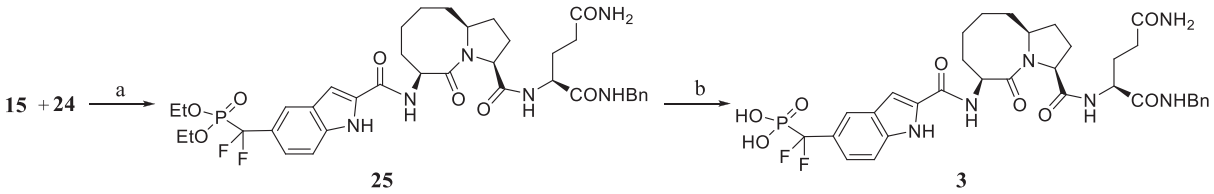

Reagents and Conditions: a. EDC-HCl, HOBt, EtN(i-Pr)$_2$, CH_2Cl_2, rt, 3 hr; b. TMSI 4.0 equiv., 0°C, 2 hr.

*(2-((3S,6S)-3-((S)-5-Amino-1-(benzylamino)-1,5-dioxopentan-2-ylcarbamoyl)-5-oxode cahydropyrrolo[1,2-a]azocin-6-ylcarbamoyl)-1H-indol-5-yl)difluoromethylphosphonic acid (**3**).* The freshly prepared amine **15** (0.2 mmol) and acid **24** (0.2 mmol) were coupled - using peptide coupling condition (3.0 equiv. HOBt. 3.0 equiv. EDC-HCl, and 4.0 equiv. EtN(i-Pr)$_2$, CH_2Cl_2 as solvent). The reaction was stirred at room temperature for 3 hr before quenching with saturated $NaHCO_3$. The aqueous layer was extracted with CH_2Cl_2 and the combined organic layers were washed with brine and dried over anhydrous sodium sulphate. The solvent was removed in vacuum and the residue was purified by flash column chromatography to yield **25** (117 mg). To a round bottom flask equipped with a magnetic stirring bar was added the purified **25** (0.15 mmol, 117 mg) and CH_2Cl_2 (5 mL). TMSI (0.7 mmol, 0.1 mL) was added at 0°C. The reaction mixture was stirred for 2 hr at 0°C. Volatile components were removed on a rotary evaporator and a mixture of MeCN-H_2O-AcOH (20 mL, 8:1:1) was added. The mixture was stirred at room temperature for 1 hr. The volatile components were removed on a rotary evaporator and the desired product was purified by reverse phase semi-preparative HPLC to give compound **3** (38 mg, 26% yield). ^{1}H NMR (300 MHz, MeOD-d4): 7.89 (s, 1H), 7.50 (d, J = 8.74 Hz, 1H), 7.45 (d, J = 8.74 Hz, 1H), 7.34–7.16 (m, 6H), 5.10–5.00 (m, 1H), 4.48–4.30 (m, 5H), 2.50–1.50 (m, 16H). ^{31}P NMR (121 MHz, MeOD-d4): 5.6 (t, J_{P-F} = 119 Hz). ESI-MS calculated for $C_{33}H_{40}F_2N_6O_8P$ $[M+H]^+$ = 717.26, Found: 717.33. Reverse phase analytical HPLC: > 95% purity.

*Synthesis of SI-108 **(4)**.*

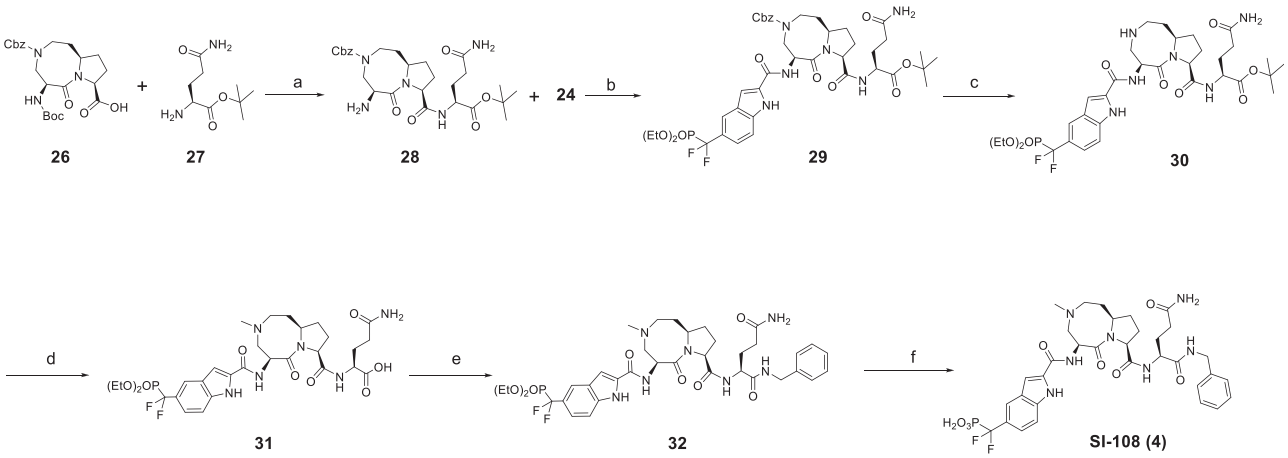

Reagents and conditions: a. 1). HATU, EtN(*i*-Pr)$_2$, DMF, rt, 1 hr; 2). TFA, DCM; b. HATU, EtN(*i*-Pr)$_2$, DMF, rt, 1 hr; c. H_2, Pd/C, MeOH; d. 1) HCHO, Sodium triacetoxyborohydride, DCE; 2). TFA, DCM; e. Benzylamine, HATU, EtN(*i*-Pr)$_2$, DMF, rt, 1 hr; f. TMSI, BSTFA, DCM.

Benzyl (5S,8S,10aR)-5-amino-8-(((S)-5-amino-1-(tert-butoxy)-1,5-dioxopentan-2-yl)carbamoyl)-6-oxooctahydropyrrolo[1,2-a][1,5] diazocine-3(4H)-carboxylate ***(28)***. HATU (418 mg, 1.1 mmol, 1.1 equiv.) was added to a solution of **26** (462 mg, 1 mmol, 1 equiv.), L-Glutamine tert-Butyl Ester **27** (202 mg, 1 mmol, 1 equiv.) and DIEA (0.52 mL, 3 mmol, 3 equiv.) in DMF (10 mL) and the resultant mixture was stirred at room temperature for 1 hr. The solution was diluted with EtOAc and washed with H_2O, saturated sodium bicarbonate aqueous solution and brine, and dried over sodium sulfate. After removal of the solvent under vacuum, the residue was dissolved in DCM (50 mL) and TFA (2.5 mL) was added. The resulting reaction was allowed to stir for one day and the solvent was removed under vacuum. The residue was purified by HPLC to afford **28** (279 mg 51% over two steps). ^{1}H NMR (400 MHz, MeOD) δ 7.44-7.33 (m, 5H), 5.33 – 5.14 (m, 2H), 4.53 (t, *J* = 8.6 Hz, 1H), 4.45 – 4.29 (m, 2H), 4.18-4.11 (m, 2H), 3.83 – 3.63 (m, 1H), 3.55 – 3.36 (m, 2H), 2.38 (tt, *J* = 7.3, 6.0 Hz, 3H), 2.28 – 2.03 (m, 3H), 2.01 – 1.72 (m, 4H), 1.50-1.44 m, 9H). UPLC-MS (ESI-MS) *m/z*: calculated for $C_{27}H_{40}N_5O_7^+$ 546.29, found $[M+H]^+$ 546.47.

Benzyl (5S,8S,10aR)-8-(((S)-5-amino-1-(tert-butoxy)-1,5-dioxopentan-2-yl)carbamoyl)-5-(5-((diethoxyphosphoryl)difluoromethyl)-1H-indole-2-carboxamido)-6-oxooctahydropyrrolo[1,2-a][1,5]diazocine-3(4H)-carboxylate ***(29)***. To a solution of **28** (200 mg, 0.37 mmol, 1 equiv.), **24** (127 mg, 0.37 mmol, 1 equiv.) and DIEA (0.19 mL, 1.1 mmoL, 3 equiv.) in DMF (5 mL) was added HATU (153 g, 0.40 mmol, 1.1 equiv.). The resultant mixture was stirred at room temperature for 1 hr and diluted with EtOAc, and was washed with H_2O, saturated sodium bicarbonate aqueous solution and brine, and dried over sodium sulfate. After removal of the solvent under vacuum, the residue was purified by flash chromatography on silica gel to afford **29** (237 mg, 74%). ^{1}H NMR (400 MHz, MeOD) δ 7.90 (s, 1H), 7.61 – 7.18 (m, 8H), 5.29 – 5.06 (m, 3H), 4.49 (t, *J* = 8.5 Hz, 1H), 4.39-4.30 (m, 2H), 4.26 – 4.08 (m, 4H), 4.01 – 3.44 (m, 4H), 2.52 – 1.62 (m, 10H), 1.50-1.43 (m, 9H), 1.29 (t, *J* = 7.1 Hz, 6H). UPLC-MS (ESI-MS) *m/z*: calculated for $C_{37}H_{46}F_2N_6O_{11}P^+$ $[M\text{-}CH_2{=}C(CH_3)_2 + H]^+$819.29, found $[M - CH_2{=}C(CH_3)_2 + H]^+$ 819.59.

Tert-butyl ((5S,8S,10aR)-5-(5-((diethoxyphosphoryl)difluoromethyl)-1H-indole-2-carboxamido)-6-oxodecahydropyrrolo[1,2-a] [1,5]diazocine-8-carbonyl)-L-glutaminate ***(30)***. To a solution of compound **29** (150 mg, 0.17 mmol) in MeOH (10 mL) was added 10% Pd-C (50 mg). The solution was stirred under 1 atm of H_2 at room temperature for 3 hours before filtering through celite and concentrating. The resulting amine was purified by HPLC to afford compound **30** (103 mg, 81%). ^{1}H NMR (400 MHz, MeOD) δ 7.91 (s, 1H), 7.56 (d, *J* = 8.7 Hz, 1H), 7.46 (d, *J* = 8.8 Hz, 1H), 7.33 (d, *J* = 0.6 Hz, 1H), 5.64 (dd, *J* = 12.1, 5.6 Hz, 1H), 4.84 – 4.67 (m, 2H), 4.39 (dd, *J* = 9.2, 5.3 Hz, 1H), 4.29 – 4.04 (m, 4H), 3.79 – 3.50 (m, 3H), 3.43 (t, *J* = 12.4 Hz, 1H), 2.53 – 2.41 (m, 1H), 2.37 (t, *J* = 7.4 Hz, 2H), 2.28 – 1.80 (m, 7H), 1.48 (s, 9H), 1.36 – 1.23 (m, 6H). UPLC-MS (ESI-MS) *m/z*: calculated for $C_{33}H_{48}F_2N_6O_9P^+$ 741.32, found $[M+H]^+$ 741.44.

((5S,8S,10aR)-5-(5-((Diethoxyphosphoryl)difluoromethyl)-1H-indole-2-carboxamido)-3-methyl-6-oxodecahydropyrrolo[1,2-a] [1,5]diazocine-8-carbonyl)-L-glutamine ***(31)***. To a 25 mL round bottom flask equipped with a magnetic stirring bar was added **30** (103 g, 0.14 mmol, 1.0 equiv), HCHO (37%, 0.06 mL, 0.70 mmol, 5.0 equiv) and DCE (5 mL). $NaBH(OAc)_3$ (59 mg, 0.28 mmol, 2.0 equiv) was added. The solution was stirred room temperature for 2 hours until LC-MS indicated the reaction was finished. Water (5 ml) was added to quench the reaction. Extracted with DCM (10 mL x 3) and dried with anhydrous sodium sulfate. Filtered and the solvent was removed under vacuum. The residual crude product was dissolved in DCM (5 ml), and TFA (2 mL) was added. The resulting mixture was stirred at room temperature until UPLC-MS detected to be finished. Most of the organic solvent was removed by evaporation, then the residue was purified by HPLC to afford **31** (60 mg, 64% yield over two steps). ^{1}H NMR (400 MHz, MeOD) δ 7.93 (s, 1H), 7.59 (d, *J* = 8.7 Hz, 1H), 7.47 (d, *J* = 8.8 Hz, 1H), 7.34 (d, *J* = 0.6 Hz, 1H), 5.63 (dd, *J* = 11.9, 5.3 Hz, 1H), 4.84 (t, *J* = 8.9 Hz, 1H), 4.75-4.71 (m, 1H), 4.56 (dd, *J* = 9.9, 4.3 Hz, 1H), 4.30 – 4.09 (m, 4H), 4.01 (t, *J* = 12.7 Hz, 1H), 3.80 (dd, *J* = 12.1, 5.4 Hz, 1H), 3.60 (d, *J* = 14.3 Hz, 1H), 3.43 (t, *J* = 12.0 Hz, 1H), 3.13 (s, 3H), 2.56-2.49 (m, 1H), 2.45 – 2.16 (m, 5H), 2.14 – 2.02 (m, 1H), 2.00 – 1.82 (m, 3H), 1.31 (t, *J* = 7.1 Hz, 6H). UPLC-MS (ESI-MS) *m/z*: calculated for $C_{30}H_{42}F_2N_6O_9P^+$ 699.27, found $[M+H]^+$ 699.05.

((2-(((5S,8S,10aR)-8-(((S)-5-amino-1-(benzylamino)-1,5-dioxopentan-2-yl)carbamoyl)-3-methyl-6-oxodecahydropyrrolo[1,2-a][1,5] diazocin-5-yl)carbamoyl)-1H-indol-5-yl)difluoromethyl)phosphonic acid (SI-108, ***4***). To a solution of acid **31** (35 mg, 0.05 mmol, 1 equiv.), benzylamine (5.4 mg, 0.05 mmol, 1 equiv.) and DIEA (46 μL, 0.15 mmoL, 3 equiv.) in DMF (3 mL) was added HATU (21 mg, 0.055 mmol, 1.1 equiv.). The resultant mixture was stirred at room temperature for 10 min and purified by HPLC to yield compound **32** (32 mg). The purified **32** (32 mg. 0.04 mmol, 1 equiv.) was dissolved in DCM (4 mL) and cooled to 0°C before adding $CF_3CON(TMS)_2$ (BSTFA) (63 mg, 0.24 mmol, 6.0 equiv) and 1M of TMS-I in DCM (0.16 mL, 0.16 mmol, 4.0 equiv). The reaction mixture was allowed to stir at 0°C for 10 min and the solvent was removed under vacuum at 0°C. The residue was dissolved in a mixed solvent of CH_3CN (1 mL), water (2 mL) and TFA (0.1 mL), and purified by HPLC to yield SI-108 (**4**, 24 mg, 65% over two steps). ^{1}H NMR (400 MHz, CD_3CN:D_2O = 1:1) δ 7.82 (s, 1H), 7.45-7.39 (m, 2H), 7.31 – 7.23 (m, 2H), 7.19 (dd, *J* = 6.0, 3.6 Hz, 4H), 5.50 – 5.28 (m, 1H), 4.67-4.48 (m, 2H), 4.25 (s, 2H), 4.22 – 4.18 (m, 1H), 3.82-3.73 (m, 1H), 3.62 – 3.51 (m, 1H), 3.44-3.37 (m, 1H), 3.24 (t, *J* = 12.2 Hz, 1H), 2.88 (s, 3H), 2.38-2.30 (m, 1H), 2.22 (t, *J* = 7.6 Hz, 2H), 2.14 – 1.92 (m, 3H), 1.87 – 1.63 (m, 4H). UPLC-MS (ESI-MS) *m/z*: calculated for $C_{33}H_{41}F_2N_7O_8P^+$ 732.27, found $[M+H]^+$ 732.44.

Synthesis of SD-109 ***(5)***.

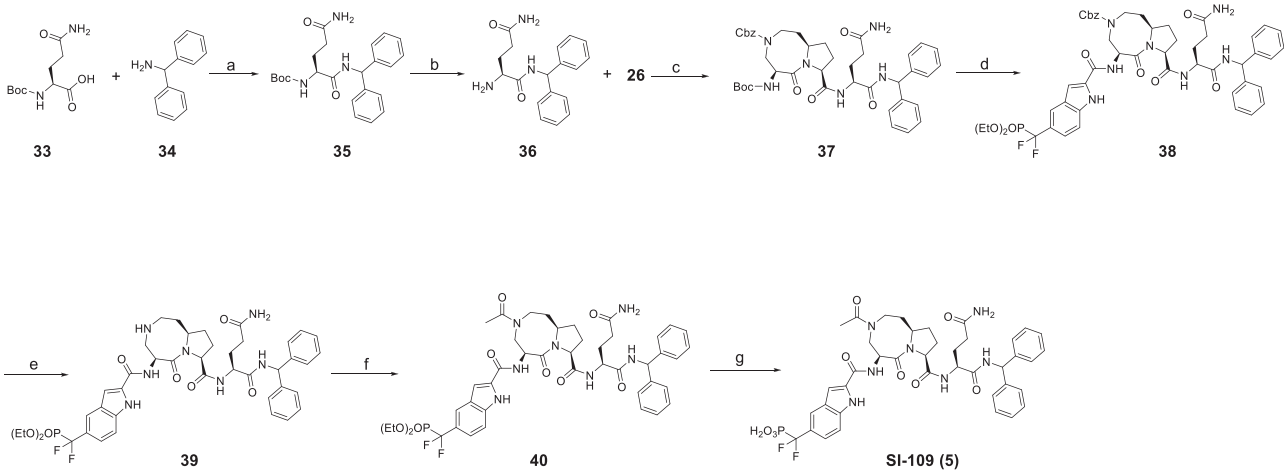

Reagents and conditions: a. HATU, EtN(*i*-Pr)$_2$, DMF, rt, 1 hr; b. TFA, DCM; c. HATU, EtN(*i*-Pr)$_2$, DMF, rt, 1 hr; d. 1) TFA, DCM; 2) **24**, HATU, EtN(*i*-Pr)$_2$, DMF, rt, 1 hr; e. H_2, Pd/C, MeOH; f. Ac_2O, EtN(*i*-Pr)$_2$, DCM; g. TMSI, BSTFA, DCM.

Tert-butyl (S)-(5-amino-1-(benzhydrylamino)-1,5-dioxopentan-2-yl)carbamate ***(35)***. To a solution of Boc-Gln-OH **33** (5.0 g, 20.3 mmol, 1 equiv.), aminodiphenylmethane hydrochloride (4.5 g, 20.3 mmol, 1 equiv.) and DIEA (10.6 mL, 60.9 mmol, 3 equiv.) in DMF (60 mL) was added HATU (8.5 g, 22.3 mmol, 1.1 equiv.) and the resulting mixture was stirred at room temperature for 1 hr. The solution was diluted with EtOAc and washed with H_2O, saturated sodium bicarbonate aqueous solution and brine, and dried over sodium sulfate. After removal of the solvent under vacuum, the residue was purified by flash chromatography on silica gel to afford compound **35** (7.3 g 87%). ^{1}H NMR (400 MHz, $CDCl_3$) δ 7.95 (d, *J* = 6.5 Hz, 1H), 7.35 – 7.23 (m, 10H), 6.36 (s, 1H), 6.21 (d, *J* = 8.2 Hz, 1H), 5.89 (d, *J* = 5.8 Hz, 1H), 5.74 (s, 1H), 4.24 (s, 1H), 2.33-2.26 (m, 1H), 2.21 – 2.11 (m, 1H), 2.09-2.00 (m, 1H), 1.92-1.87 (m, 1H), 1.43 (s, 9H). ^{13}C NMR (101 MHz, $CDCl_3$) δ 175.42, 171.02, 156.26, 141.50, 141.32, 128.63, 127.44, 80.10, 56.92, 53.75, 31.91, 29.10, 28.31.

(S)-2-Amino-N1-benzhydrylpentanediamide ***(36)***. TFA (5 mL) was added slowly to a solution of compound **35** (3 g) in DCM (50 mL) and the resulting reaction solution was stirred at room temperature for 6 hours and then evaporated. The residue consisting of **36** was directly used in the next step without purification.

Benzyl (5S,8S,10aR)-8-(((S)-5-amino-1-(benzhydrylamino)-1,5-dioxopentan-2-yl)carbamoyl)-5-((tert-butoxycarbonyl)amino)-6-oxooctahydropyrrolo[1,2-a][1,5]diazocine-3(4H)-carboxylate ***(37)***. HATU (1.59 g, 4.2 mmol, 1.1 equiv.) was added to a solution of **26** (1.75 g, 3.8 mmol, 1 equiv.), **36** (1.61 g, 3.8 mmol, 1 equiv.) and DIEA (1.98 mL, 11.4 mmol, 3 equiv.) in DMF (15 mL) and the resulting mixture was stirred at room temperature for 1 hr. The solution was diluted with EtOAc and washed with H_2O, saturated sodium bicarbonate aqueous solution and brine, and dried over sodium sulfate. After removal of the solvent under vacuum, the residue was purified by flash chromatography on silica gel to afford **37** (2.4 g 84 %). ^{1}H NMR (400 MHz, MeOD) δ 7.46 – 7.39 (m, 2H), 7.38 – 7.19 (m, 13H), 6.16-6.15 (m, 1H), 5.20-5.18 (m, 2H), 4.74 – 4.57 (m, 1H), 4.56 – 4.37 (m, 2H), 4.25-4.23 (m, 1H), 3.87 – 3.35 (m, 4H), 2.55 – 2.28 (m, 2H), 2.27 – 1.58 (m, 8H), 1.46 (s, 9H). UPLC-MS (ESI-MS) *m/z*: calculated for $C_{41}H_{51}N_6O_8P^+$ 755.38, found $[M+H]^+$ 755.52.

Diethyl ((2-(((5S,8S,10aR)-8-(((S)-5-amino-1-(benzhydrylamino)-1,5-dioxopentan-2-yl)carbamoyl)-6-oxodecahydropyrrolo[1,2-a][1,5]diazocin-5-yl)carbamoyl)-1H-indol-5-yl)difluoromethyl)phosphonate ***(39)***. TFA (3 mL) was added slowly to a solution of **37** (2 g, 2.65 mmol) in DCM (30 mL) at room temperature and the resulting reaction solution was stirred at the same temperature for 6 hours and then evaporated. The crude product was directly used in the next step without purification. To a solution of the crude product of the previous step (2.65 mmol, 1 equiv.), **24** (0.92 g, 2.65 mmol, 1 equiv.) and DIEA (1.39 mL, 7.95 mmoL, 3 equiv.) in DMF (15 mL) was added HATU (1.1 g, 2.91 mmol, 1.1 equiv.). The resulting mixture was stirred at room temperature for 1 hr and diluted with EtOAc, and was washed with H_2O, saturated sodium bicarbonate aqueous solution and brine, and dried over sodium sulfate. After removal of the solvent under vacuum, the residue was purified by flash chromatography on silica gel to afford **38**. To a solution of the obtained **38** in MeOH (60 mL) was added 10% Pd-C (200 mg). The solution was stirred under 1 atm of H_2 at room temperature for 3 hours before filtering through celite and concentrating. The resulting amine was purified by HPLC to afford compound **39** (1.73 g, 77% over three steps). ^{1}H NMR (400 MHz, MeOD) δ 7.92 (s, 1H), 7.57 (d, *J* = 8.7 Hz, 1H), 7.46 (d, *J* = 8.8 Hz, 1H), 7.38 – 7.31 (m, 5H), 7.30 – 7.24 (m, 6H), 6.19 (s, 1H), 5.61 (dd, *J* = 12.1, 5.6 Hz, 1H), 4.78 (t, *J* = 8.9 Hz, 1H), 4.70-4.66 (m, 1H), 4.59 (dd, *J* = 9.5, 5.0 Hz, 1H), 4.29 – 4.05 (m, 4H), 3.72-3.61 (m, 2H), 3.54 (t, *J* = 12.6 Hz, 1H), 3.42 (t, *J* = 12.4 Hz, 1H), 2.45 – 2.27 (m, 3H), 2.24 – 2.01 (m, 3H), 2.00 – 1.70 (m, 4H), 1.29 (td, *J* = 7.1, 3.2 Hz, 6H). UPLC-MS (ESI-MS) *m/z*: calculated for $C_{42}H_{51}F_2N_7O_8P^+$ 850.35, found $[M+H]^+$ 850.37.

((2-(((5S,8S,10aR)-3-acetyl-8-(((S)-5-amino-1-(benzhydrylamino)-1,5-dioxopentan-2-yl)carbamoyl)-6-oxodecahydropyrrolo[1,2-a][1,5]diazocin-5-yl)carbamoyl)-1H-indol-5-yl)difluoromethyl)phosphonic acid (SI-109, ***5***). Acetic anhydride (24 mg, 0.24 mmoL, 2 equiv.) and DIEA (61 μL, 0.35 mmol, 3 equiv.) were added to a solution of **39** (100 mg, 0.12 mmol, 1 equiv.) in DCM (5 mL). The resulting

reaction mixture was stirred for half an hour and then was evaporated and the residue was purified by flash chromatography on silica gel to afford **40**. SI-109 (**5**) was prepared from compound **40** by similar procedures as those for SI-108 (**4**) from **32**. The overall yield for these two steps was 69%. ^{1}H NMR (400 MHz, CD_3CN:D_2O = 1:1) δ 7.90 (s, 1H), 7.56-7.52 (m, 1H), 7.48-7.46 (m, 1H), 7.35-7.21 (m, 11H), 6.07-6.06 (m, 1H), 5.11-5.02 (m, 1H), 4.42 – 4.23 (m, 3H), 3.95 – 3.80 (m, 1H), 3.77 – 3.53 (m, 2H), 3.49 – 3.37 (m, 1H), 2.32-2.26 (m, 2H), 2.19-2.14 (m, 4H), 2.11-2.01 (m, 2H), 1.96 – 1.58 (m, 5H). UPLC-MS (ESI-MS) *m/z*: calculated for $C_{40}H_{45}F_2N_7O_9P^+$ 836.30, found $[M+H]^+$ 836.43.

Synthesis of SD-36 ***(6)***.

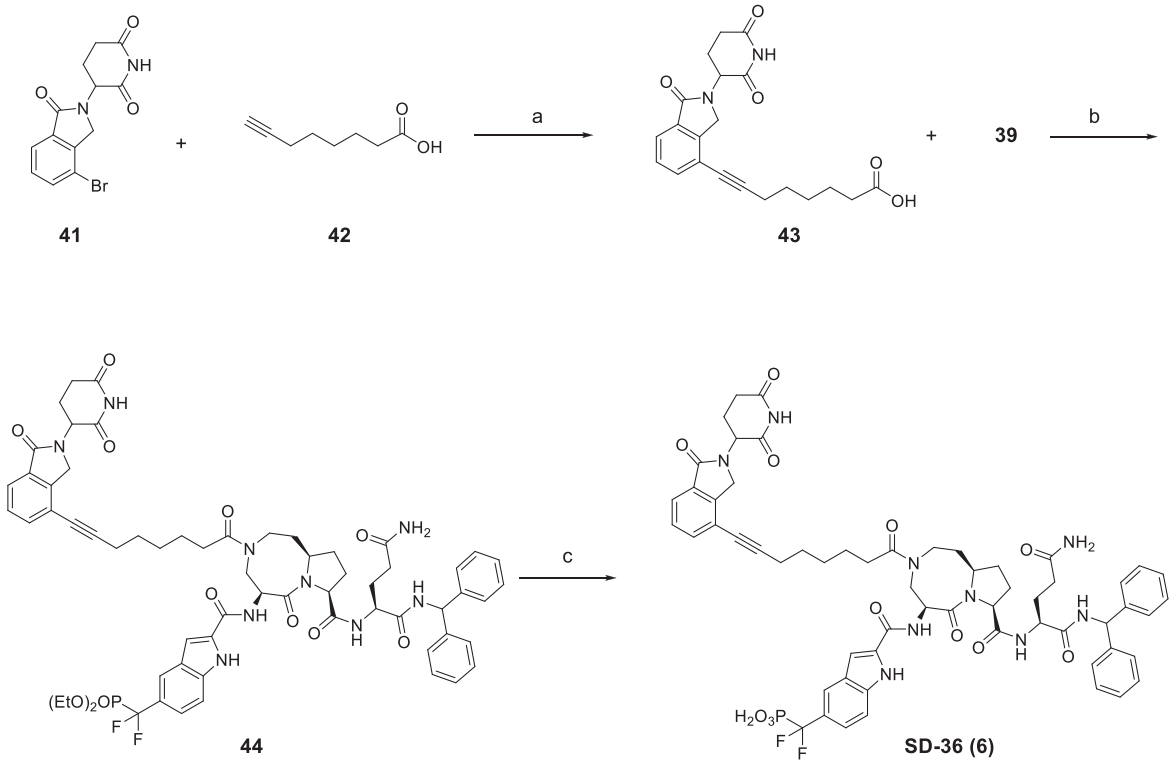

Reagents and conditions: a. $Pd(PPh_3)Cl_2$, CuI, DMF/TEA, 80°C, 3 hr; b. HATU, DIEA, DMF; c. TMSI, BSTFA, DCM.

8-(2-(2,6-Dioxopiperidin-3-yl)-1-oxoisoindolin-4-yl)oct-7-ynoic acid ***(43)***. Trimethylamine (10 mL) was added to a mixture of compound **41** (1.3 g, 4.0 mmol, 1 equiv.), oct-7-ynoic acid **42** (0.56 g, 4.0 mmol, 1 equiv.), CuI (154 mg, 0.8 mmol, 0.2 equiv) and $Pd(PPh_3)_2Cl_2$ (282 mg, 0.4 mmol, 0.1 equiv) in DMF (10 mL). The resulting mixture was purged and refilled with argon three times and stirred at 70-80°C for 3 hr under argon. The reaction mixture was then cooled to room temperature and evaporated to remove most of the solvent. The residue was purified by HPLC to yield the **43** (1.18 g ,76%). ^{1}H NMR (400 MHz, DMSO) δ 11.99 (s, 1H), 10.99 (s, 1H), 7.77 – 7.68 (m, 1H), 7.68 – 7.59 (m, 1H), 7.52 (t, *J* = 7.6 Hz, 1H), 5.15 (dd, *J* = 13.3, 5.0 Hz, 1H), 4.46 (d, *J* = 17.7 Hz, 1H), 4.33 (d, *J* = 17.7 Hz, 1H), 2.97-2.88 (m, 1H), 2.63-2.59 (m, 1H), 2.53 – 2.47 (m, 3H), 2.24 (t, *J* = 7.2 Hz, 2H), 2.13 – 1.94 (m, 1H), 1.78 – 1.27 (m, 6H). ^{13}C NMR (101 MHz, DMSO) δ 174.90, 173.32, 171.45, 168.14, 144.23, 134.52, 132.46, 129.05, 123.05, 119.32, 96.73, 76.91, 52.14, 47.47, 34.07, 31.68, 28.32, 28.25, 24.50, 22.83, 19.14. UPLC-MS (ESI-MS) *m/z*: calculated for $C_{21}H_{23}N_2O_5^+$ 383.16, found $[M+H]^+$ 383.28.

Diethyl ((2-(((5S,8S,10aR)-8-(((S)-5-amino-1-(benzhydrylamino)-1,5-dioxopentan-2-yl)carbamoyl)-3-(8-(2-(2,6-dioxopiperidin-3-yl)-1-oxoisoindolin-4-yl)oct-7-ynoyl)-6-oxodecahydropyrrolo[1,2-a][1,5]diazocin-5-yl)carbamoyl)-1H-indol-5-yl)difluoromethyl)phosphonate ***(44)***. HATU (295 mg, 0.77 mmol, 1.1 equiv.) was added to a solution of **39** (600 mg, 0.71 mmol, 1 equiv.), **43** (270 g, 0.71 mmol, 1 equiv.) and DIEA (0.37 mL, 2.12 mmol, 3 equiv.) in DMF (10 mL) and the resulting mixture was stirred at room temperature for 1 hr. The solution was diluted with EtOAc and washed with H_2O, saturated sodium bicarbonate aqueous solution and brine, and dried over sodium sulfate. After removal of the solvent under vacuum, the residue was purified by flash chromatography on silica gel to afford **44** (702 mg 82 %). ^{1}H NMR (400 MHz, MeOD:$CDCl_3$ = 1:1) δ 7.90 (s, 1H), 7.76 – 7.66 (m, 1H), 7.57-7.51 (m, 2H), 7.47 – 7.35 (m, 2H), 7.33 – 7.19 (m, 11H), 6.27 – 6.06 (m, 1H), 5.33 – 4.87 (m, 2H), 4.55 – 4.37 (m, 4H), 4.26 – 3.75 (m, 7H), 3.71 – 3.26 (m, 2H), 2.90 – 2.71 (m, 2H), 2.67 – 1.85 (m, 14H), 1.83 – 1.47 (m, 8H), 1.29 (t, *J* = 7.1 Hz, 6H).

((2-(((5S,8S,10aR)-8-(((S)-5-amino-1-(benzhydrylamino)-1,5-dioxopentan-2-yl)carbamoyl)-3-(8-(2-(2,6-dioxopiperidin-3-yl)-1-oxoisoindolin-4-yl)oct-7-ynoyl)-6-oxodecahydropyrrolo[1,2-a][1,5]diazocin-5-yl)carbamoyl)-1H-indol-5-yl)difluoromethyl)phosphonic acid (SD-36, ***6***). To a round bottom flask was added **44** (500 mg, 0.41 mmol, 1.0 equiv) and CH_2Cl_2 (40 mL). The solution was cooled to 0°C before adding $CF_3CON(TMS)_2$ (635 mg, 2.5 mmol, 6.0 equiv) and 1M of TMS-I in DCM (1.65 mL, 1.65 mmol, 4.0 equiv). The

reaction mixture was allowed to stir at 0°C for 10 min and the solvent was removed under vacuum at 0°C. The residue was dissolved in a mixed solvent of CH_3CN (5 mL), water (5 mL) and TFA (0.3 mL), and purified by HPLC to yield SD-36 (**6**, 420 mg, 88%). ^{1}H NMR (400 MHz, CD_3CN:D_2O = 1:1) δ δ 7.90-7.85 (m, 1H), 7.73 – 7.59 (m, 1H), 7.56 – 7.36 (m, 4H), 7.35 – 7.05 (m, 11H), 6.06-6.03 (m, 1H), 5.12 – 4.87 (m, 2H), 4.48 – 4.19 (m, 5H), 3.98 – 3.49 (m, 3H), 3.36 – 3.24 (m, 1H), 2.88 – 2.64 (m, 2H), 2.61 – 2.23 (m, 7H), 2.21 – 1.99 (m, 4H), 1.94 – 1.35 (m, 11H). UPLC-MS (ESI-MS) *m/z*: calculated for $C_{59}H_{63}F_2N_9O_{12}P^+$ 1158.43, found $[M+H]^+$ 1158.60.

*Synthesis of SD-36Me **(7)**.*

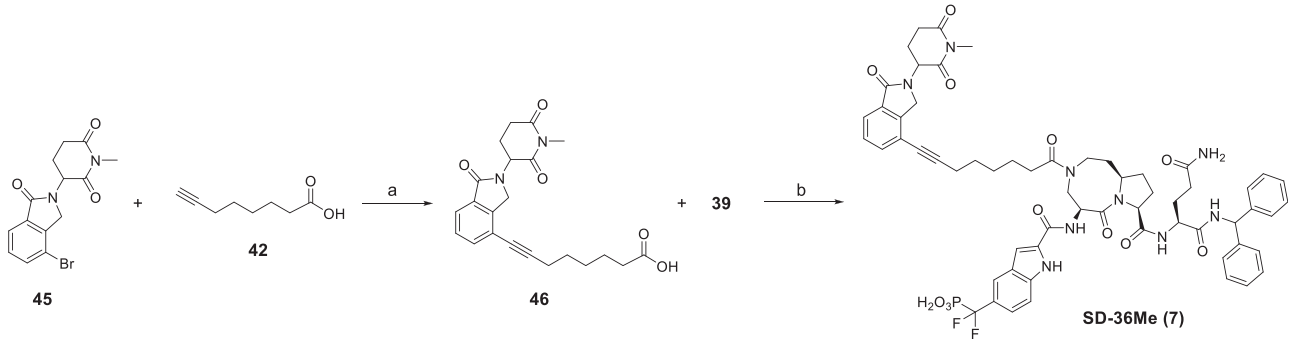

Reagents and conditions: a. $Pd(PPh_3)Cl_2$, CuI, DMF/TEA, 80°C, 3 hr; b. HATU, DIEA, DMF; c. TMSI, BSTFA, DCM.

*8-(2-(1-Methyl-2,6-dioxopiperidin-3-yl)-1-oxoisoindolin-4-yl)oct-7-ynoic acid **(46)**.* Compound **46** was synthesized using a similar method as for compound **43** with a yield of 71%. ^{1}H NMR (400 MHz, DMSO) δ 10.04 (s, 1H), 7.74 – 7.68 (m, 1H), 7.61 (dd, *J* = 7.6, 0.8 Hz, 1H), 7.49 (t, *J* = 7.6 Hz, 1H), 5.22 (dd, *J* = 13.5, 5.1 Hz, 1H), 4.43 (d, *J* = 17.7 Hz, 1H), 4.32 (d, *J* = 17.6 Hz, 1H), 3.08 – 2.91 (m, 4H), 2.78-2.74 (m, 1H), 2.55 – 2.36 (m, 3H), 2.24-2.19 (m, 2H), 2.10 – 1.97 (m, 1H), 1.60 – 1.38 (m, 6H). ^{13}C NMR (101 MHz, DMSO) δ 174.90, 172.25, 171.00, 168.22, 144.20, 134.47, 132.36, 128.90, 123.00, 119.35, 96.59, 76.86, 52.59, 47.36, 34.03, 31.80, 28.28, 28.19, 26.93, 24.46, 22.11, 19.08. UPLC-MS (ESI-MS) *m/z*: calculated for $C_{22}H_{25}N_2O_5^+$ 397.18, found $[M+H]^+$ 397.31.

*((2-(((5S,8S,10aR)-8-(((S)-5-amino-1-(benzhydrylamino)-1,5-dioxopentan-2-yl)carbamoyl)-3-(8-(2-(1-methyl-2,6-dioxopiperidin-3-yl)-1-oxoisoindolin-4-yl)oct-7-ynoyl)-6-oxodecahydropyrrolo[1,2-a][1,5]diazocin-5-yl)carbamoyl)-1H-indol-5-yl)difluoromethyl)phosphonic acid (SD-36Me, **7**).* SD-36Me (**7**) was synthesized using a similar method as for SD-36 employing **46** as starting material and the yield was 61% over two steps. ^{1}H NMR (400 MHz, CD_3CN:D_2O = 1:1) δ 7.88 (d, *J* = 16.1 Hz, 1H), 7.72 – 7.59 (m, 1H), 7.56 – 7.36 (m, 4H), 7.35 – 7.06 (m, 11H), 6.06-6.03 (m, 1H), 5.12 – 4.87 (m, 2H), 4.45 – 4.20 (m, 5H), 3.98 – 3.50 (m, 3H), 3.37 – 3.22 (m, 1H), 3.08 – 2.94 (m, 3H), 2.88 – 2.73 (m, 2H), 2.61 – 2.37 (m, 4H), 2.34-1.99 (m, 7H), 1.95-1.81 (m, 2H), 1.79 – 1.40 (m, 9H). UPLC-MS (ESI-MS) *m/z*: calculated for $C_{60}H_{65}F_2N_9O_{12}P^+$ 1172.45, found $[M+H]^+$ 1172.45.

*Synthesis of SD-45FL **(8)**.*

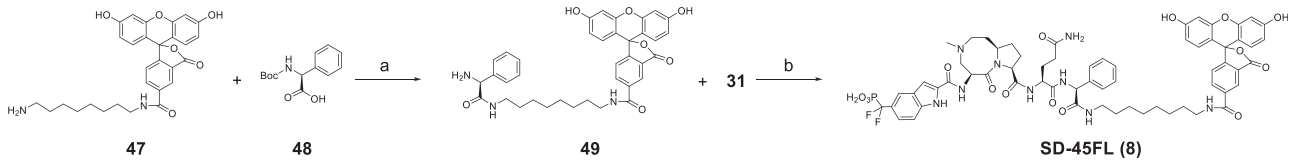

Reagents and conditions: a. 1) HATU, DIEA, DMF; 2) TFA, DCM; b. 1) HATU, DIEA, DMF; 2) TMSI, BSTFA, DCM.

*((2-(((5S,8S,10aR)-8-(((S)-5-amino-1-(((S)-2-((8-(3',6'-dihydroxy-3-oxo-3H-spiro[isobenzofuran-1,9'-xanthene]-5-carboxamido)octyl)amino)-2-oxo-1-phenylethyl)amino)-1,5-dioxopentan-2-yl)carbamoyl)-3-methyl-6-oxodecahydropyrrolo[1,2-a][1,5]diazocin-5-yl)carbamoyl)-1H-indol-5-yl)difluoromethyl)phosphonic acid (SD-45FL, **8**).* To a solution of **47** (50 mg, 0.1 mmol, 1 equiv.), (S)-2-((tert-butoxycarbonyl)amino)-2-phenylacetic acid **48** (25 mg, 0.1 mmol, 1 equiv.), and DIEA (0.05 mL, 0.3 mmoL, 3 equiv.) in DMF (3 mL) was added HATU (42 mg, 0.11 mmol, 1.1 equiv.). The resulting mixture was stirred at room temperature for 1 hr and diluted with EtOAc, and was washed with H_2O, saturated sodium bicarbonate aqueous solution and brine, and dried over sodium sulfate. After removal of the solvent under vacuum, the residue was dissolved in DCM (5 mL) and TFA (1 mL) was added. The resulting mixture was stirred at room temperature for 3 hr. After removal of most of the organic solvent, the residual was purified by HPLC to afford compound **49** (32 mg, 50% over two steps). To a solution of the **49** (32 mg, 0.05 mmol, 1 equiv.), **31** (35 mg, 0.05 mmol, 1 equiv.) and DIEA (0.025 mL, 0.15 mmoL, 3 equiv.) in DMF (3 mL) was added HATU (21 g, 0.055 mmol, 1.1 equiv.). The resultant mixture was stirred at room temperature for 1 hr and directly purified by HPLC. SD-45FL (**8**) was prepared using a similar method as for SD-36 (**7**) from **44** and the yield was 65% over two steps. ^{1}H NMR (400 MHz, CD_3CN) δ 8.30 (s, 1H), 8.06 (dd, *J* = 8.0, 1.5 Hz, 1H), 7.82 (s, 1H), 7.45-7.39 (m, 2H), 7.34 – 7.08 (m, 7H), 6.75-6.72 (m, 2H), 6.65-6.63 (m, 2H), 6.55-6.53 (m, 2H), 5.37 (s, 1H), 5.24 (s, 1H), 4.63-4.51 (m, 2H),

4.34-4.28 (m, 1H), 3.79-3.55 (m, 2H), 3.45 – 3.19 (m, 4H), 3.13-3.06 (m, 1H), 2.98-2.91 (m, 1H), 2.87 (s, 3H), 2.32-2.21(m, 3H), 2.11 – 1.93 (m, 3H), 1.86 – 1.65 (m, 4H), 1.56 – 1.39 (m, 2H), 1.33 – 1.01 (m, 10H). UPLC-MS (ESI-MS) *m/z*: calculated for $C_{63}H_{70}F_2N_9O_{15}P^{2+}$ 630.73, found $[M+2H]^{2+}$ 630.92.

Expression and Purification of STAT Proteins

Complementary DNA fragments for the corresponding human STAT proteins: STAT1(residues 132-713), STAT2 (138-702) and STAT3 (127-688) were cloned into a pHis-SUMO vector; and STAT4 (133-705), STAT5A (136-705) and STAT5B (138-710) were cloned into a pHis-MBP-TEV vector and STAT6 (113-658) was cloned into a pHis-TEV vector. All clones were expressed in Luria broth overnight at 20°C in Rosetta DE3 cells. Proteins were purified from the cleared cell lysate using Ni-NTA resin (Qiagen) and cleaved overnight in the presence of either SUMO or TEV protease, then passed over a second Ni-NTA column to remove the tag and protease. They were then concentrated and loaded onto a Superdex 200 column (GE Healthcare) pre-equilibrated with 10 mM HEPES 7.5, 100mM NaCl, 2 mM DTT (STAT1); 50 mM Tris pH 8.5, 150 mM NaCl, and 1 mM DTT (STAT3); or 25 mM HEPES 7.5, 200 mM NaCl, 1 mM DTT (STAT2 ,4, 5A and 5B). For binding assays, His-SUMO-STAT3 was not cleaved prior to loading onto a Superdex 200 column pre-equilibrated with 50 mM Tris pH 8.0, 150 mM NaCl, 0.1% NP-40, 1 mM DTT and 10% glycerol. After cleavage, STAT6 was diluted to 75 mM NaCl with 25 mM HEPES 7.5, 1 mM DTT and loaded onto a HiTrap SP column (GE Healthcare). Protein was eluted with a salt gradient, concentrated and loaded onto a Superdex 200 pre-equilibrated with 20mM HEPES 7.0 , 200mM NaCl, 1 mM DTT.

Crystallization and Structure Determination of STAT3-SI109 and STAT3-SD36

STAT3 was concentrated to 6.25 mg/mL and incubated with a 1.2-fold molar excess of SI-109 or SD-36 for 3 hours at 4°C. Crystals were grown by sitting drop vapor diffusion against well solution containing 10% PEG 3350 and 100 - 150 mM ammonium nitrate at 4°C. Crystals were cryoprotected in mother liquor containing 20% ethylene glycol prior to flash freezing in liquid nitrogen. Data were collected at the Life Sciences Collaborative Access Team beamline 21-ID-D at the Advanced Photon Source, Argonne National Laboratory. Data were processed with HKL2000 (Otwinowski and Minor, 1997) and the structures were solved by molecular replacement using Phaser (McCoy et al., 2007) with PDB 3CWG as a search model. The structures were iteratively refined with Buster (Bricogne et al., 2017) and fit with COOT (Emsley et al., 2010). Coordinates and geometric restraints for the compounds were generated in Grade (Smart et al., 2017). The complexes crystallized in space group P41212 with 1 molecule in the asymmetric unit. Residues 136-687 were modeled with the exception of the following missing loop regions: 181-191, 372-378 and 419-429. Prior to deposition, the structures were validated with Molprobity (Chen et al., 2010b) and the PDB validation server (wwPDB Validation Server) (Table S5).

Molecular Modeling

The crystal structure of STAT3 (pY705) with DNA (PDBID: 1BG1(Becker et al., 1998)) was used to model the binding pose of AA-115 with STAT3. The chain A of STAT3 (pY705) from the crystal structure was extracted and the protons on the protein were added using the "protonate 3D" module in MOE (CCG, 2018) by setting the physiological pH value at 7.0. AA-115 was drawn and optimized using MOE for the docking calculation using the GOLD program (version 5.2) (Jones et al., 1997). In the docking calculation, the center of the binding site in STAT3 was set at V637 and the radius of the binding site was defined as 13 Å. A maximum number of 200,000 operations were performed on a population of 5 islands of 100 individuals in each genetic algorithm run. Operator weights for crossover, mutation and migration were set to 95, 95 and 10 respectively. GoldScore was used as the fitness function to rank the docked poses. The top ranked pose was considered as the binding model to suggest the location of the 8-membered ring suitable for coupling to the cereblon ligand in the STAT3 degrader design.

Fluorescence Polarization (FP) Assay

The FP assay was performed to determine dissociation constants (K_d) for the interactions between STAT3 SH2 domain binder SD-45FL and STATs, in which 5 nM of SD-45-FL, the 5-FAM labeled SI-109, was incubated with serially diluted recombinant STAT proteins in FP buffer (50 mM NaCl, 10 mM HEPES pH 7.5, 1 mM EDTA pH 8.0, 0.01% Triton X-100, 2 mM DTT). FP was measured after 1 hour of incubation on a Tecan Infinite microplate reader. Data are fit using one-site specific with 4-parameter nonlinear regression curve fitting model. K_d values were determined from the binding isotherm derived from curves of mP vs protein concentrations. For the competitive assays, STAT3 recombinant protein (25 nM) was first combined with SD-45-FL (2.5 nM) for 5 min, then added to the serially diluted compounds. FP was measured after 1 hour of incubation at room temperature. IC_{50} values of SD-45-FL displacement were calculated by nonlinear regression analysis using GraphPad Prism software. The K_i values of competitive inhibitors were calculated as described (Cer et al., 2009).

Biolayer Interferometry (BLI) Assay

Purified recombinant STAT proteins were biotinylated using the EZ-Link biotinylation reagent (Thermo Fisher Scientific). Briefly, protein and biotinylation reagent were mixed with 1:1 molar ratio in PBS at 4°C. Low biotinylation reagent concentration was applied to avoid protein over-biotinylation. These reaction mixtures were incubated at 4°C for 2 hours to allow completion of the reaction. Reaction mixture was then dialyzed using 10K MWCO dialysis cassettes (Thermo Fisher Scientific) to remove unreacted biotinylation reagent.

BLI experiments were performed using an OctetRED96 instrument from ForteBio. All assays were run at 30°C with continuous 1000 RPM shaking. PBS with 0.1% BSA, 0.01% Tween-20 and 1% DMSO was used as the assay buffer. Biotinylated STAT proteins were tethered on Super Streptavidin (SSA) biosensors (ForteBio) by dipping sensors into 10 μg/mL protein solutions. Average saturation response levels of 10-15 nm were achieved in 15 minutes for all STAT proteins. Sensors with proteins tethered were washed in assay buffer for 10 minutes to eliminate nonspecifically bound protein molecules and establish stable base lines before starting association-dissociation cycles with test compound. DMSO only references were included in all assays. Raw kinetic data collected were processed in the Data Analysis software provided by the manufacturer using double reference subtraction in which both DMSO only reference and inactive reference were subtracted. Resulting data were analyzed based on 1:1 binding model from which k_{on} and k_{off} values were obtained and then K_d values were calculated.

Nuclear Extract Preparation and STAT DNA Binding Activity Assay

To prepare nuclear extract, cells were harvested by centrifuging at 500 × g for 5 minutes, washed with PBS twice, and then incubated in Buffer A (10 mM HEPES pH 7.9, 10 mM KCl, 0.1 mM EDTA, 0.1 mM EGTA, 1 mM DTT plus PhoSTOP and Complete Mini protease inhibitor cocktail) on ice for 15 min, after which 10 % solution of Nonidet NP-40 (final conc: 0.5%) was added and the tube was vigorously vortexed for 10 sec. The homogenate was centrifuged at 500 × *g* for 5 minutes. The nuclear pellet was resuspended in ice-cold Buffer B (20 mM HEPES pH 7.9, 0.4 M NaCl, 1 mM EDTA, 1 mM EGTA, 1 mM DTT plus PhoSTOP and Complete Mini protease inhibitor cocktail) and the tube was vigorously rocked at 4°C for 15 min on a shaking platform. The nuclear extract was centrifuged at 5,000 × *g* for 5 minutes at 4°C and the supernatant was aliquoted for DNA binding assay. The protein concentration was determined using the Bio-Rad Protein Assay.

The DNA binding activities for activated STAT1, STAT3, STAT5A and STAT5B were determined using the TransAM STAT Family ELISA Kits following the manufacturer's protocol. Essentially, 30 μL of Complete Binding Buffer was added to each well followed by adding 20 μL (5 μg) of nuclear extracts diluted in Complete Binding Buffer. After 1 hour incubation at room temperature, the wells were washed 3 times with 1X Wash Buffer. Then 100 μL of the 1:1000 diluted STAT antibodies was added to each well and incubated at room temperature for 1 hour on an orbital shaker. After washing, 100 μL of the diluted HRP-conjugated secondary antibody was added to each well and incubated at room temperature for 1 hour. The wells were washed with 1X Wash Buffer four times, then 100 μL of Developing Solution was added to each well and incubated at room temperature for 2-10 minutes for color development. Then 100 μL of Stop Solution was added to each well to stop the reaction. Plate was read on a Tecan Infinite microplate reader at 450 nm with a reference wavelength of 655 nm.

Site-Directed Mutagenesis of Human STAT3

pCMV6-STAT3-Myc-DDK plasmid expressing Myc and DDK (equivalent to Flag) tagged human STAT3 (Origene, RC215836) was used as template for site-directed mutagenesis of STAT3 SH2 domain. QuikChange II Site-Directed Mutagenesis Kit (Agilent Technologies, #200524) was used following the manufacturer's instruction. Fifty nanograms of pCMV6-STAT3-Myc-DDK were used as template in each 50 μl reaction. Each PCR reaction was performed as follows: 95°C for 30 seconds; 16 cycles of 95°C for 30 seconds, 55°C for 1 minute and 68°C for 8 minutes. The mutagenesis was confirmed by Sanger sequencing performed at the University of Michigan Sequencing Core. The expression of tagged mutant STAT3 protein was confirmed by transient transfection of MDA-MB-231 cells followed by immunoblotting.

The primers (custom-synthesized at the Thermo Fisher Scientific) used for mutagenesis are in Table S6.

Plasmid Purification and Transient Transfection

Plasmids were purified with QIAprep Spin Miniprep Kit (Qiagen, #27106) according to the manufacturer's instruction. Plasmid transfection was performed using FuGENE 6 (Promega) following the manufacturer's instructions. MDA-MB-231 cells were plated in 12-well plates at ~50% confluency and grown overnight. Before transfection, the culture medium was changed to fresh complete growth medium without antibiotics. One microgram of plasmid DNA was used for each well. The ratio of FuGENE 6 to DNA was 4 μl:1 μg. One to two days after transfection, the cells were used for treatment.

Silencing of *CRBN* Expression

SMARTvector lentiviral particles for human *CRBN* shRNA and empty vector control were from Dharmacon. Cells were spinfected with viral particles at 2:1 cells/viral particles in the presence of 8 μg/ml of polybrene (Sigma/Aldrich) for 1 hour at 500 × *g* and room temperature. Transduced cells were then transferred to fresh complete growth medium, and selected with 1 μg/mL puromycin (Invitrogen) 48 hours after transduction. The expression of CRBN in puromycin-resistant cells was determined by immunoblotting.

Cell Viability Assay

Cell viability assay was performed as described previously (Bai et al., 2017). Cells seeded in 384-well white plates (Corning Costar) were incubated with serially diluted compounds for 4 days. Cell viability was determined using the CellTiter-Glo Luminescent Cell Viability Assay (Promega) following the manufacturer's instruction. Data points were fit with a four-parameter equation to generate a concentration-response curve. When plotting concentration-response fitting curves, DMSO controls were defined as the lowest doses of serial diluted compounds and set as 0 on x-axis. IC_{50} values were calculated using a nonlinear regression analysis of the mean ± SD from at least triplicates for each biological assay.

Luciferase Reporter Assay

For the reporter assays, 1000-2000 cells were seeded in 384-well white plate (Corning Costar). Two duplicate plates were set up: one for luciferase reporter assay and one for CellTiter-Glo cell viability assay. Four to six hours later, drugs were added to each well and cultured for 24 or 48 hours. Firefly luciferase and Renilla luciferase activities were determined using the Luciferase Assay Reagent and Renilla Luciferase Assay (Promega), respectively. The luminescence signal was measured with a Tecan Infinite microplate reader. The raw luminescent light units were normalized to cell numbers determined by cell viability assay to account for cell number.

Cell Cycle and Annexin V Apoptosis Assays

For cell cycle analysis, cells were collected after treatment, washed twice with cold PBS (Hyclone), fixed in 50% ethanol overnight, and stained with PI (50 μg/ml, Sigma) plus 0.2 μg/ml of DNase-free RNase A (Qiagen) for 1 hr at 4°C. For the Annexin V apoptosis assay, cells were collected at the end treatment, washed with cold PBS, and stained with the Annexin V-FLOUS Staining Kit (Roche) following the manufacturer's instructions. All flow cytometric analyses were performed at the University of Michigan Flow Cytometry Core.

Overexpression of c-Myc in SU-DHL-1 Cells

Myc-DDK-tagged c-Myc expressing and control lentiviral particles were from OriGene. SU-DHL-1 cells were spinfected with viral particles at 1:1 cells/viral particles ratio in the presence of 8 μg/ml of polybrene for 1 hour at 500 × *g* and room temperature. Transduced cells were then transferred to fresh complete growth medium. Twenty-four hours after transduction, the cells were seeded in duplicate 384-well white plates (Corning Costar) and treated with DMSO or SD-36 for up to 3 days for caspase-3/7 activity assay and cell viability assay or 12-well plates and treated for immunoblotting analysis.

Caspase 3/7 Activity Assay

Cellular caspase-3/7 activity was determined using Caspase-Glo 3/7 Assay kit (Promega) following the manufacturer's instructions. Cells were seeded in duplicate plates and treated with drugs. At the end of treatment, luminescence signals for caspase-3/7 activity and cell viability by CellTiter-Glo Luminescent Cell Viability Assay (Promega) were recorded using a Tecan Infinity microplate reader. The raw Caspase 3/7 signal was normalized to cell numbers determined by cell viability assay (DMSO-treated cells set as 100%). This normalized caspase 3/7 signal was expressed as % of the average of DMSO control, which was set as 100%.

Mitochondrial OXPHOS Complex Enzyme Activity Assay

Cells were treated with DMSO or SD-36 for 24 hours and crude mitochondria was isolated using the Mitochondria Isolation Kit (Thermo Fisher Scientific, #89874) following the manufacturer's instruction. Mitochondrial OXPHOS Complex I (NADH dehydrogenase) enzyme activity and Complex II (succinate-coenzyme Q reductase) enzyme activity were determined using the Complex I Enzyme Activity Microplate Assay Kit (Abcam, ab109721) and Complex II Enzyme Activity Microplate Assay Kit (Abcam, ab109908), respectively. In the enzymatic assays, reactions without cell fraction lysis were included as controls. Plates were read in a kinetic mode every 20 sec for 30-60 min on a Tecan Infinite microplate reader at room temperature. The enzymatic activity was expressed as the change in absorbance (milli OD, mOD) per minute, which was calculated by fitting the initial linear portion of each kinetic curve. Relative enzymatic activity was presented as % of the average of DMSO controls.

Co-immunoprecipitation (Co-IP)

MOLM-16 cells were collected after treatment with SD-36, washed with PBS, and lysed in 1X Cell Lysis Buffer (Cell Signaling Technology, #9803). Cell lysates were centrifuged at 13,000 rpm for 10 min at 4°C and the supernatant was collected. For IP, 200 μg of total protein lysate was used for each IP condition, and 10% of the total lysate was used as input. Cell lysates were pre-cleared with Sepharose-conjugated rabbit IgG (Santa Cruz). Fifty microliters of Sepharose beads-conjugated STAT3 antibody or the rabbit IgG control (Cell Signaling Technology) were added to lysates and incubated for 8 hours at 4°C on a rotator. The beads were then washed 3 times with 1X Cell Lysis Buffer and the immunoprecipitated proteins were eluted by incubating with 1X NuPAGE LDS Sample Buffer (Thermo Fisher Scientific) at 95°C for 10 min and resolved by SDS-PAGE followed by Immunoblotting.

Immunoblotting

Cells were lysed Cell Lysis Buffer (Cell Signaling Technology, #9803), resolved by SDS-PAGE NuPAGE gel (Thermo Fisher Scientific), and transferred to a PVDF membrane (Millipore). For native PAGE, NativePAGE 4-16% Bis-Tris Protein Gels (Invitrogen, #IBN1002BOX) were used. Membranes were blocked for 1 hour using 5% Blotting-Grade Blocker (#1706404, Bio Rad) in Tris-buffered saline with Tween 20 (TBST, Pierce). Antibodies used are listed in the Key Resource Table. The PVDF membranes were incubated with SuperSignal West Pico Chemiluminescent Substrate (Thermo Fisher Scientific) for 1 min and films were developed using a X-ray film developer.

Pervanadate (PV) Rreatment

Nonspecific tyrosine phosphatase inhibitor PV has been shown to induce the tyrosine phosphorylation of STAT proteins (Haque et al., 1995, 1997). PV is freshly prepared by mixing 0.1 mM sodium orthovanadate (Biovision, #9471-5) with 0.2 M hydrogen peroxide (Sigma, H1009) at 1:1 (v/v) at room temperature for 15 min. Then hydrogen peroxide is inactivated by adding a small amount of

catalase (Sigma, C40) and incubates for 5 min. The mixture is centrifuged at 15,000 rpm for 5 min, and the supernatant fraction (PV) is used for treatment. The cells were treated with 0.5-50 μM for 30 min.

Quantitative Reverse Rranscriptase-Polymerase Chain Reaction (qRT-PCR)

RNA was isolated using the RNeasy Mini Kit (Qiagen #74104). Reverse transcriptase reaction (RT) was performed with 1 μg of total RNA using the High-Capacity RNA-to-cDNA Kit (Thermo Fisher Scientific) and followed by polymerase chain reaction (PCR) using TaqMan Gene Expression Master Mix or Power SYBR Green Master Mix (Thermo Fisher Scientific) on a QuantStudio 7 Flex Real-Time PCR System (Thermo Fisher Scientific). The relative abundance of gene expression was calculated using the comparative C_T method which compares the Ct value of target gene to GAPDH or ACTB ($2^{\Delta\Delta CT}$). TaqMan primer/probe sets are listed in the Key Resource Table. SYBR green primers are in Table S6.

Transcriptomic Profiling

Total RNA was purified using RNeasy Mini Kit (Qiagen, #74104) following the manufacturer's instructions. RNA was assessed for quality using the TapeStation (Agilent). Samples with RINs (RNA Integrity Numbers) $\geq$8 were ribosomal RNA depleted using Ribo-Zero rRNA Removal Kit (Human/Mouse/Rat) (cat# MRZH11124, Illumina). The rRNA depleted samples were then prepared using the TruSeq mRNA Sample Prep v2 kit (Catalog #s RS-122-2001, RS-122-2002, Illumina). Where the entire fraction of 0.1-3 μg of rRNA depleted total RNA was fragmented and copied into first strand cDNA using reverse transcriptase and random primers. The 3 prime ends of the cDNA were then adenylated and adapters were ligated. One of the adapters that was ligated had a 6 nucleotide barcode that was unique for each sample and this allowed us to sequence more than one sample in each lane of a HiSeq flow cell (Illumina). The products were purified and enriched by PCR to create the final cDNA library. Final libraries were checked for quality and quantity by TapeStation (Agilent) and qPCR using Kapa's library quantification kit for Illumina Sequencing platforms (catalog # KK4835, Kapa Biosystems). They were clustered on the cBot (Illumina) and sequenced with 16 samples per lane in a 50 cycle single end High Output mode using version 4 reagents and HiSeq Control Software version 2.2.68 according to manufacturer's protocols. Demultiplexing and Fastq file generation was done using bcl2fastq version 2.17.1.14. RNA-seq data are deposited at Gene Expression Omnibus (GEO) as GSE131358.

Raw data were normalized into reads per kilobase per million (RPKM) values. Genes with the average RPKM values less than 1.00 were removed from the analysis. All the RPKM values were then added to one before the analysis to avoid singularity in the fold change calculations. The MultiplotPreprocess module from the GenePattern (Reich et al., 2006) website were used to calculate the overall fold changes and the corresponding p-values in paired comparison. The data were plotted using the R program.

GSEA was performed using the GSEA program (Subramanian et al., 2005) and the Molecular Signature Database (v6.1) (Liberzon et al., 2011, 2015) (http://www.broad.mit.edu/gsea/) using the GSEA preranked function. Differential expression of SD-36 versus DMSO treatment was used to generate the ranked list file. In the analysis, 1000 permutations were applied to determine the significance of the enrichment for the gene sets.

Proteomic Profiling

Cultured cell lines and xenograft tumors samples were lysed in RIPA buffer (Sigma, #R0278). Cell lysis samples (75 μg/condition) were proteolysed and labeled with TMT 10-plex Isobaric Label Reagent (Thermo Fisher Scientific, #90110) essentially following manufacturer's protocol. Briefly, upon reduction and alkylation of cysteines, the proteins were precipitated by adding 6 volumes of ice-cold acetone followed by overnight incubation at −20°C. The precipitate was spun down, and the pellet was allowed to air dry. The pellet was resuspended in 0.1M TEAB and digested overnight with trypsin (1:50; enzyme:protein) at 37°C with constant mixing using a thermomixer. The TMT 10-plex reagents were dissolved in 41 μl of anhydrous acetonitrile and labeling was performed by transferring the entire digest to the TMT reagent vial and incubating it at room temperature for 1 hour. Reaction was quenched by adding 8 μl of 5% hydroxylamine and further 15 min incubation. Labeled samples were mixed together, and dried using a vacufuge. An offline fractionation of the combined sample (~200 μg) into 10 fractions was performed using high pH reversed-phase peptide fractionation kit according to the manufacturer's protocol (Pierce; Cat #84868). Fractions were dried and reconstituted in 12 μl of 0.1% formic acid/2% acetonitrile in preparation for LC-MS/MS analysis.

In order to obtain superior accuracy in quantitation, we employed multinotch-MS3 (McAlister et al., 2014) which minimizes the reporter ion ratio distortion resulting from fragmentation of co-isolated peptides during MS analysis. Orbitrap Fusion (Thermo Fisher Scientific) and RSLC Ultimate 3000 nano-UPLC (Dionex) was used to acquire the data. The sample (2 μl) was resolved on a PepMap RSLC C18 column (75 μm i.d. x 50 cm; Thermo Scientific) at the flow-rate of 300 nl/min using 0.1% formic acid/acetonitrile gradient system (2-22% acetonitrile in 150 min; 22-32% acetonitrile in 40 min; 20 min wash at 90% followed by 50 min re-equilibration) and direct spray into the mass spectrometer using EasySpray source (Thermo Fisher Scientific). The mass spectrometer was set to collect one MS1 scan (Orbitrap; 60K resolution; AGC target $2x10^5$; max IT 100 ms) followed by data-dependent, "Top Speed" (3 seconds) MS2 scans (collision induced dissociation; ion trap; NCD 35; AGC $5x10^3$; max IT 100 ms). For multinotch-MS3, top 10 precursors from each MS2 were fragmented by HCD followed by Orbitrap analysis (NCE 55; 60K resolution; AGC $5x10^4$; max IT 120 ms, 100-500 m/z scan range).

Proteome Discoverer (v2.1; Thermo Fisher) was used for data analysis. MS2 spectra were searched against SwissProt human protein database (release 2015-11-11; 42084 sequences) using the following search parameters: MS1 and MS2 tolerances were set to 10 ppm and 0.6 Da, respectively; carbamidomethylation of cysteines (57.02146 Da) and TMT labeling of lysine and N-termini

of peptides (229.16293 Da) were considered static modifications; oxidation of methionine (15.9949 Da) and deamidation of asparagine and glutamine (0.98401 Da) were considered variable. Identified proteins and peptides were filtered to retain only those that passed $\leq$1% FDR threshold. Quantitation was performed using high-quality MS3 spectra (Average signal-to-noise ratio of 20 and <30% isolation interference).

Statistical Analyses

For tumor growth kinetics, DNA binding, cell cycle and apoptosis analyses, data were presented as mean ± SEM. For concentration-response cell viability, FP binding and luciferase reporter assays, data were plotted as mean ± SD and fitted to a sigmoidal curve by nonlinear regression. Differences in mean values between groups were analyzed by two-sided Student's *t* test. All statistical analyses were performed using GraphPad Prism 7.

DATA AND CODE AVAILABILITY

X-ray crystallography coordinates of SI-109 and SD-36 in complex with recombinant STAT3 protein are deposited to the Protein DataBank (PDB). The accession number for SI-109:STAT3 reported in this paper is PDB: 6NUQ and the accession number for SD-36:STAT3 is PDB: 6NJS. All RNA-seq raw data are deposited at the Gene Expression Omnibus (GEO). The accession number for the RNA-seq data reported in this paper is GEO: GSE131358.